Preparation and application of composite phase change materials stabilized by cellulose nanofibril-based foams for thermal energy storage

Shen, Zhenghui; Kwon, Soojin; Lee, Hak Lae; Toivakka, Martti; Oh, Kyudeok

Published in:
International Journal of Biological Macromolecules

DOI:
10.1016/j.ijbiomac.2022.10.075

Published: 01/12/2022

Document Version
Accepted author manuscript

Preparation and application of composite phase change materials stabilized by cellulose nanofibril-based foams for thermal energy storage

Zhenghui Shen [a,b], Soojin Kwon [c], Hak Lae Lee [b], Martti Toivakka [d], Kyudeok Oh [e *]

[a] Beijing Key Laboratory for Theory and Technology of Advanced Battery Materials, School of Materials Science and Engineering, Peking University, Beijing 100871, P. R. China

[b] Program in Environmental Materials Science, Department of Agriculture, Forestry and Bioresources, College of Agriculture and Life Sciences, Seoul National University, Seoul 08826, Korea

[c] Department of Forest Biomaterials, North Carolina State University, Raleigh, North Carolina 27695, United States

[d] Laboratory of Natural Materials Technology, Åbo Akademi University, Turku 20500, Finland

[e] Department of Bio Based Materials, Chungnam National University, 99 Daehak-ro, Yuseong-gu, Daejeon, 34134, South Korea

*Corresponding author: Kyudeok Oh (kyudeok.oh@cnu.ac.kr)

Tel: +82-42-821-5759, Fax: +82-42-821-6159

Funding: This work was supported by research fund of Chungnam National University.

Abstract: The leakage issue and inferior heat conduction of organic phase change materials (PCMs) limit their actual applications. In present study, cellulose nanofibril (CNF)-based foams were prepared as the porous scaffolds for polyethylene glycol (PEG) and paraffin wax (Pw) to prevent their leakage, and multiwalled carbon nanotubes (CNTs) were incorporated to improve the heat transfer performance. The prepared foams had low density (<67.3 kg/m^3) and high porosity (>94.5%). Selective chemical modifications of nanocellulose foams enhanced their shape-stability and compatibility with PCMs. The highly porous foam structure and favorable compatibility resulted in PCM loading levels (93.63% for PEG and 91.77% for Pw) and negligible PCM leakage (<2%). CNTs improved the heat transfer performance of PCMs, as evidenced by the improved thermal conductivities and boosted temperature rises during solar heating. Meanwhile, the composite PCMs exhibited improved thermal stability over the control. PEG-based composite PCM exhibited phase change enthalpy of 143 J/g with melting temperature of 25.2 °C**;** Pw-based composite PCM exhibited phase change enthalpy of 184 J/g with melting temperature of 53.4 °C**.** Novel PCM sandwich structures based on these composite PCMs and a thermoelectric generator was designed and displayed promising potential for solar energy harvesting and utilization.

Keywords: cellulose nanofibril, phase change materials, multiwalled carbon nanotubes, form-stability, heat transfer enhancement, thermal energy storage

1. Introduction

Latent heat storage (LHS) owing to its advantages of high volumetric energy storage density and small temperature swings represents a promising strategy for expanding the utilization of renewable energies and coping with the energies tension. The fulfillment of a LHS process relies on the reversible phase transitions of the energy storage medium (i.e. the phase change materials, PCMs), where heat can be stored during heating and used later [1]. PCMs are typically categorized into inorganic, organic and eutectic ones, and each type has their pros and cons. Eutectics PCM systems compromises at least two different kinds of PCMs and show complexity for composition design and property tuning. Inorganic PCMs, with salt hydrates as the most representative family, exhibited the advantages of high energy storage capacity, relatively higher thermal conductivity, and inexpensiveness, widely extending their applications in both domestic and industrial applications [2]. Nevertheless, salt hydrates exhibit devastating drawbacks such as phase segregation and supercooling during the charging and discharging processes, which severely harm their energy storage performance in cyclic charging and discharging and timely release of the stored energy [3,4]. On the contrary, organic PCMs do not suffer from phase segregation, have no or little supercooling, and exhibit broad ranges of working temperatures, non-corrosivity and chemical stability properties, making them promising candidates for a variety of practical applications [5].

Polyethylene glycol (PEG) and paraffin wax (Pw) as typical organic PCMs provide favorable characteristics for LHS such as high heat of fusion, negligible supercooling, nontoxicity and non-corrosivity [6–8]. However, their solid-liquid phase transition features make them suffer from the large volume change in their phase transitions, which causes the leakage issue and limit its wide applications [9,10]. Therefore, fabricating form-stable composite PCMs is of great importance for ensuring their efficient and reliable uses for LHS systems. Porous materials, as the supporting matrix to stabilize PCMs, could absorb the liquid PCMs into the pores and prevent their leakage in the melting process. Compared to other approaches like core-shell microencapsulation, using porous scaffolds to prepare form-stable composite PCMs is simple and effective. A variety of supporting skeletons, such as porous carbon-based (e.g., expanded graphite, graphene aerogels, carbon nanotube sponges), mineral-based

(e.g., expanded perlite and expanded vermiculite), metal-based (e.g., aluminum and copper foams), polymer-based (e.g., polystyrene and polyurethane foams) and silica-based materials (e.g., silica aerogels) [11], have been used to fabricate composite PCMs with stable form during their phase transitions. However, most of these porous materials usually require harsh or energy-intensive preparations and costly precursors. Moreover, the majority of these materials are not sustainable. Therefore, the development of sustainable and high-performance porous scaffolds for organic PCMs is of great importance to actual applications and provokes great interest to researchers.

Cellulose as the most abundant natural polymers on earth represents a promising material for numerous fields because of its fascinating properties like biodegradability, renewability, recyclability, safety and low price [12–14]. Cellulose surface has abundant hydroxyl groups, and these functional groups endow the feasibility of various chemical modifications through oxidation, esterification, polymer grafting, etc. [15]. Importantly, cellulose chains readily form entangled networks even in low concentration aqueous suspensions [16], making it quite easy to prepare porous structures from cellulose suspension after removing the solvent by drying. One thing to consider is the compatibility between the foam scaffolds and PCMs, and this can be easily fulfilled by tuning the surface chemistry of cellulose foams as explained above. Compared to conventional PCM scaffolds like silica aerogels and carbon aerogels, cellulose-based porous supporting materials exhibit advantages of ease of preparation, superior environmentally friendliness, and cost-effectiveness. Moreover, cellulose materials are of low density and low thermal expansion coefficient [17]. These superior properties of cellulose are making them promising starting materials for next generation foams and aerogels.

Another intrinsic drawback of organic PCMs that hinders their LHS performance is the low thermal conductivity [18]. In practical uses, PCMs with high thermal conductivity are preferred as their charging process can be shorter and cost-effective [19]. To enhance the thermal conductivity of PCMs, various thermally conductive fillers including metal nanoparticles, carbon spheres, graphite, graphene nanoplatelets, carbon fibers, carbon nanotubes can be used [19,20]. In the present study, carbon nanotubes (CNTs) are selected due to their ultrahigh thermal conductivity and high aspect ratio [21]. Carbon nanomaterials, however, suffer from severe aggregation due to the high surface area and the strong van der

Waals force between these nanoparticles [22]. Instead of environmentally unfriendly surfactants, nanocellulose can be applied as the dispersing agent for carbon nanomaterials thanks to their amphiphilic nature. Green nanocellulose facilitates the dispersion of carbon nanomaterials via hydrophobic-hydrophobic interactions and intercalation effect, and this, does not harm the intrinsic thermal properties of carbon materials [23]. Therefore, the preparation of nanocellulose/carbon foam as the supporting matrix for PCMs provides a solution for addressing the two intrinsic drawbacks of organic PCMs simultaneously.

In this work, form-stable composite PCMs with enhanced thermal conduction performance were prepared by using nanocellulose based foam as a supporting matrix. To improve the shape-stability of foams and their compatibility with PCMs, silane agent-induced chemical modification was carried out, and the effect of surface chemistry tuning on PCM stabilization was explored. Multiwalled CNTs as the heat transfer enhancers were applied in the preparation of porous supporting foams. Herein, nanocellulose serves not only the skeleton of the foam but also the dispersing agent of CNTs. The morphologies, structures, phase change properties, thermal stability, and thermal reliability of the prepared composite PCMs were investigated. In particular, leakage testing was performed to examine the form-stability of the prepared composite PCMs. Moreover, special PCM sandwich structures were designed and tested for absorption and conversion of solar energy. By addressing the leakage issue and the inferior thermal conduction of PEG and Pw, their efficient applications for LHS would be expanded. Besides, the interest of using naturally occurring polymers such as polysaccharides for stabilizing PCMs for sustainable energy applications is expected to increase.

2. Experimental

2.1 Materials

Bleached eucalyptus kraft pulp (BEKP) was the starting material to prepare CNF. (3-Aminopropyl)trimethoxysilane (APTMS) and Methyltrimethoxysilane (MTMS) silylation reagent, paraffin wax (Pw), and polyethylene glycol (PEG) PCMs were purchased from Sigma-Aldrich (St. Louis, MO, USA). Hydrochloric acid used to regulating pH was purchased from Duksan Pure Chemicals Co., Ltd. (Ansan-city, Korea). Multiwalled CNTs in powder form were

purchased from Research Nanomaterials, Inc. (Houston, TX, USA). Filter paper (quantitative ashless, 11 cm in diameter; ADVANTEC, Tokyo, Japan) was used for leakage testing of the prepared composite PCMs. Detailed information of the materials is available in Table 1.

Table 1. Detailed information of the materials used in the experiments.

Material	Specification	Role	Provider
BEKP	Commercial grade	CNF starting mateial	Moorim Paper Co., Ltd., Korea
APTMS	purity 97%	Silylation agent	Sigma-Aldrich, USA
MTMS	purity 98%	Silylation agent	Sigma-Aldrich, USA
Pw	Mw=436	Hydrophobic PCM	Sigma-Aldrich, USA
PEG	Mw=1000	Hydrophilic PCM	Sigma-Aldrich, USA
HCl	1 N, laboratory grade	PH regulator	Duksan Pure Chemicals Co., Ltd, Korea
Multiwalled CNTs	purity >95%, outer diameter 10–20 nm	Thermal conductivity enhancer	Research Nanomaterials, Inc., USA
Filter paper	Quantitative ashless, 11 cm in diameter	Leakage testing substrate	ADVANTEC, Japan

2.2 Methods

2.2.1 Preparation of CNF

CNF was prepared by grinding a 2 wt% pulp suspension 30 times using a Super Masscolloider grinder (Masuko Sangyo Co., Ltd., Kawaguchi-city, Japan) and the entire grinding process consumed about 8 hours. The gap between the two grinding plates was −80 μm, and the grinding speed was 1,500 rpm. The zeta potential of the resulting CNF, determined using a Malvern Zetasizer (Nano-ZS, Malvern Instruments Ltd., Worcestershire, UK), was −34.8 ± 0.5 mV. The charge density of the CNF, according to a titration method, was 0.16 meq/g CNF.

2.2.2 Preparation of CNF/CNT composites

CNF/CNT composites were prepared by homogenizing CNTs in a 0.5% CNF suspension using an Ultra-Turrax T50 homogenizer (Janke and Kunkel, IKA-Labortechnik, Staufen, Germany) at 10,000 rpm for 60 min. The homogenized suspensions were then centrifuged with a centrifugal (Combi R514, Hanil Scientific Inc., Gimpo, Korea) at 9,000 rpm for 30 min to obtain the CNF/CNT composites. Different amounts of CNTs (10, 20, 30, and 50 wt%, based

on CNF) were used for the preparation, and the resulting composites were coded as CNF/CNT_{10}, CNF/CNT_{20}, CNF/CNT_{30}, and CNF/CNT_{50}, where the subscript indicates the dose (wt%) of CNTs.

2.2.3 Preparation of foams

CNF-based foams were prepared by freeze-drying the corresponding suspensions. To tune the surface chemistry of CNF, the pH of a 2% CNF suspension was adjusted to 4 by using HCl. Then silane chemical APTMS or MTMS was added to the CNF suspension at the mass ratio of 2:1, and the silylation reaction was continued while mixing at 1,500 rpm at room temperature for 2 h. The silylated CNF suspension was then stored in a refrigerator (4°C) to minimize the possible cracking and shrinkage of foams during subsequent freeze-drying [24]. The precooled CNF suspension was frozen in liquid nitrogen, followed by a 72 h freeze-drying (FD8518 freeze dryer, Ilshin Lab. Co., Ltd., Yangju-city, Korea). Foams were cured at 120 °C for 3 h to ensure the completion of silylation. The CNF/CNT foams were similarly prepared by freeze-drying the corresponding silylated CNF/CNT suspensions. When APTMS was used as the silane agent, the prepared foams were labeled as CNF_{APTMS}, CNF_{APTMS}/CNT_{10}, CNF_{APTMS}/CNT_{20}, CNF_{APTMS}/CNT_{30}, and CNF_{APTMS}/CNT_{50}, where the subscript denotes the dose (wt%) of CNTs based on the dry weight of CNF. When MTMS was used as the silane agent, the prepared foams were labeled as CNF_{MTMS}, CNF_{MTMS}/CNT_{10}, CNF_{MTMS}/CNT_{20}, CNF_{MTMS}/CNT_{30}, and CNF_{MTMS}/CNT_{50}, where the subscript denotes the dose (wt%) of CNTs based on the dry weight of CNF.

The apparent densities of the foams were calculated from their weights and dimensions, which were determined with a digital caliper (Absolute Origin, iGaging, San Clemente, CA, USA). The porosity (P, %) of the foams was calculated from their apparent densities and skeleton densities according to Equation (1) [25].

$$P = \left(1 - \frac{\rho_a}{\rho_s}\right) \times 100\% \quad (1)$$

where ρ_a is the apparent density of the foam (kg/m^3) and ρ_s is the density of the foam skeleton (kg/m^3).

For silylated CNF foams, $\rho_s = \frac{1}{\frac{w_{CNF}}{\rho_{CNF}} + \frac{w_{Silane}}{\rho_{Silane}}}$ (2)

and for silylated CNF/CNT foams, $\rho_s = \frac{1}{\frac{w_{CNF}}{\rho_{CNF}} + \frac{w_{Silane}}{\rho_{Silane}} + \frac{w_{CNT}}{\rho_{CNT}}}$ (3)

where w_{CNF}, w_{Silane}, and w_{CNT} are the weight fractions (%) of CNF, silane agent, and CNTs in the foams, respectively. ρ_{CNF} was fixed at 1500 kg/m^3, ρ_{APTMS} was fixed at 1027 kg/m^3, ρ_{MTMS} was fixed at 1900 kg/m^3, and ρ_{CNT} was fixed at 2100 kg/m^3.

2.2.4. Preparation of Composite PCMs

Composite PCMs were prepared by impregnating the prepared foams with molten PCM under 1-bar vacuum for 6 h. Excess PCM on the sample surface was carefully removed using filter paper. The prepared Composite PCMs were named according to the type of the used PCM and foam. For example, the obtained PEG-based Composite PCMs were coded as CNF_{APTMS}-PEG, CNF_{APTMS}/CNT_{10}-PEG, CNF_{APTMS}/CNT_{20}-PEG, CNF_{APTMS}/CNT_{30}-PEG, and CNF_{APTMS}/CNT_{50}-PEG when APTMS silylated foams were used. Analogously, the obtained Pw-based Composite PCMs were coded as CNF_{MTMS}-Pw, CNF_{MTMS}/CNT_{10}-Pw, CNF_{MTMS}/CNT_{20}-Pw, CNF_{MTMS}/CNT_{30}-Pw, and CNF_{MTMS}/CNT_{50}-Pw when MTMS silylated foams were used. The PCM fraction of prepared Composite PCMs was calculated according to Equation (4):

$$C = \left(\frac{w_b - w_a}{w_b}\right) \times 100\% \quad (4)$$

where w_a is the foam weight before impregnation with PCM (g) and w_b is the foam weight after impregnation with PCM (g) (i.e., the weight of prepared Composite PCMs).

2.2.5 Characterizations

The morphologies of CNF, CNT, and CNF/CNT composites were studied by energy-filtering transmission electron microscopy (LIBRA 120, Carl Zeiss, Oberkochen, Germany). The structures of foams and Composite PCMs were investigated by field-emission scanning electronic microscopy (FE-SEM; Auriga; Carl Zeiss, Oberkochen, Germany). Water contact angle (WCA) measurements were performed using a drop shape analyzer (DSA100, Krüss GmbH, Hamburg, Germany).

Leakage testing of PCM samples was performed as follows. For PEG-based Composite PCMs, they were placed on a filter paper, then heated in an oven at 50 °C for 30 min. For Pw-

199 based Composite PCMs, they were placed on a filter paper, then heated in an oven at 70 °C for
200 30 min. The area of leaked PCM on filter paper was recorded by a digital camera. The leakage
201 percentage (%) of PCM was calculated according to Equation (5):

202 $$L = \left(\frac{m_a - m_b}{m_a}\right) \times 100\% \quad (5)$$

203 where m_a is the sample weight before the leakage test (g) and m_b is the sample weight after
204 the leakage test (g).

205 Fourier transform-infrared spectroscopy (FT-IR, Thermo Scientific, Waltham, MA, USA)
206 was used to record the IR spectra of samples. A D8 Advance diffractometer (Bruker, Germany)
207 with Cu kα1 radiation (wavelength λ = 1.5418 Å) operating at 40 kV and 40 mA was used to
208 obtain the X-ray diffraction (XRD) patterns of samples. Differential scanning calorimetry (DSC,
209 Discovery DSC, TA Instruments Inc., New Castle, DE, USA) was employed to investigate the
210 phase change properties of samples. Samples were heated from 0 °C to the targeted temperature
211 (70 °C for PEG and 80 °C for Pw) at a temperature ramping rate of 5°C/min, followed by a
212 cooling process to 25 °C at the same rate. A thermogravimetric analyzer (Discovery TGA, TA
213 Instruments Inc.) was used to study the thermal stability of samples over the temperature range
214 of 40–600 °C at a heating rate of 10 °C/min under 20 mL/min of nitrogen gas purge. The heat
215 transfer performance of samples was investigated as follows. A thermocouple (Electronic
216 Temperature Instruments Ltd., Worthing, UK) was used to determine the real-time temperature
217 variations of samples under the heating of a solar simulator (CEL-HXF300-T3, Ceaulight,
218 Beijing, China) The temperatures of samples were collected by a ThermaData® logger
219 (Electronic Temperature Instruments Ltd.) and exported using ThermaData® Studio software
220 (version 5.1.4, Electronic Temperature Instruments Ltd.). The thermal reliabilities of PCM
221 samples were investigated by comparing their phase change properties before and after 100
222 melting/freezing cycles. The thermal conductivity of PCM samples was measured following a
223 laser flash method. Disk-shaped samples were prepared, and their dimensions and weights were
224 measured for determining their densities. Then the thermal conductivity of samples was
225 calculated using Eq. (6) [26]:

226 $$k = \alpha \cdot C_p \cdot \rho \quad (6)$$

where κ is the thermal conductivity [W/(m·K)], α represents the thermal diffusivity (mm^2/s), C_P denotes the specific heat capacity [J/(g·K)] and ρ is the density of pellets (g/cm^3).

The application potential of the prepared composite PCM for thermal energy storage and conversion was evaluated by using the designed PCM sandwich structures based on the differences between the phase change performances of PEG and Pw. As illustrated in Fig.1., Pw-based composite PCMs were positioned on the top (hot side), a thermoelectric generator (TEG, SP1848-27145 SA, Shenzhen Chuangxin Microelectronics Co., Ltd., China) was positioned in the middle and PEG-based composite PCMs were attached to the bottom of TEG, respectively. The thermoelectric materials in the TEG is Bismuth Telluride. The dimension of TEG was about 40 mm×40 mm×3.4 mm, operating temperature ranges from –40 ºC to 150 ºC. The top side of the assembled sandwich-like structures was heated by the solar simulator, and the light intensity of the solar simulator was 469 mW/cm^2 at a working current of 14 A. The voltage generated by TEG was monitored by a 6½-Digit USB multimeter (2100 Series, Keithley Instruments, Inc., Cleveland, OH, USA).

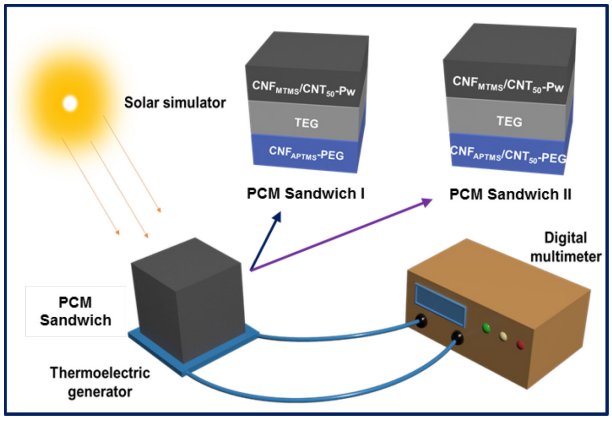

Fig. 1. Schematic illustrating the solar-heat-electricity system based on novel PCM sandwich structures.

3. Results and discussion

3.1 Effect of nanocellulose surface chemistry on PCM shape-stabilization

Surface chemistry plays a critical role in the compatibility between two materials. In other words, host and guest materials with good affinity are likely to contribute to more compatible composites. One of the research aims of this work is to address the leakage issue of PCMs by using CNF-based foams as the supporting material; thus, the surface chemistry of nanocellulose skeleton should be carefully considered as well as the porous structure of nanocellulose foams. In the present study, silane chemicals including APTMS and MTMS were used to tune the surface chemistry of CNF. The reaction mechanism between silane chemicals and CNF is schematically illustrated in Fig.2a. In the silylation process, silane chemicals were hydrolyzed to silanol and reacted with the hydroxyl groups of nanocellulose to form an interlaced network [25], which would consequently enhance the foam-stability. The chemical structures of APTMS and MTMS are shown in Fig.2b and Fig.2c, respectively. Regarding the fact that APTMS has a hydrophilic amine group while MTMS has hydrophobic methyl groups on their structures, each of them would impart different surface chemistry to CNF-based foams. The 3D network structure of CNF foam is mainly dictated by hydrogen bonding and physical entanglement between adjacent cellulose nanofibrils, which leads to poor mechanical properties of such foams. Especially, cellulose nanofibers absorb water and swell under wet or humid conditions owing to their hygroscopic nature, leading to the deterioration of network bonding between adjacent fibers and then a loss of foam strength [27,28]. Therefore, although CNF has a good affinity with PEG thanks to their abundant hydroxyl groups, surface modification of CNF by APTMS-induced chemical crosslinking was conducted to enhance the shape-stability of foams while retaining their intrinsic affinity with PEG. Considering Pw is hydrophobic, CNF was hydrophobically modified by MTMS to improve the affinity between CNF-based foams and Pw. Such surface chemistry modifications are expected to have a positive effect on the shape-stability of the resulting composite PCMs.

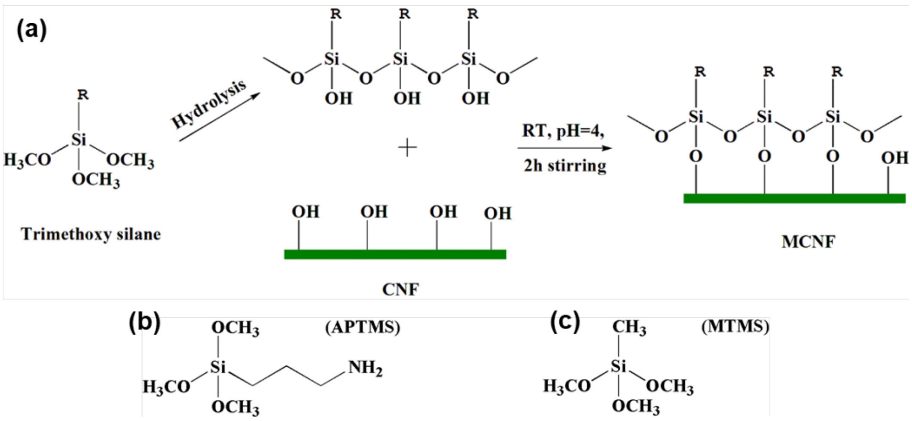

Fig. 2. (a) Chemistry tuning of CNF using trimethoxy silane and the involved reaction mechanism, (b) chemical structure of APTMS, and (c) chemical structure of MTMS.

Water contact angle (WCA) measurements were performed to quantitively investigate the hydrophilicity of the prepared foams. As shown in Fig. S1a, it was difficult to measure the WCA of pristine CNF foam as the foam surface quickly collapsed upon contact with water, which is ascribed to the hygroscopic nature of cellulose materials. CNF_{APTMS} foam absorbed water quickly due to its hydrophilicity and porous structure while the foam remained intact (Fig. S1b), indicating successful hydrophilic treatment and the enhanced foam shape-stability. CNT_{MTMS} foam, however, repels water and prevents its absorption and penetration (Fig. S1c). The measured WCA of CNT_{MTMS} foam was greater than 130° (Fig. S2), indicating strong hydrophobicity. The shape-stability of pristine CNF foam, CNF_{APTMS} foam, and CNF_{MTMS} foam was tested, and the results are shown in Figs. S1d–f. As expected, pristine CNF foam collapsed into pieces and lost its original shape during mixing with water, while the modified CNF foams maintained their structures after mixing. Although these results indicate that by suitable chemical modification both the surface chemistry and shape-stability of nanocellulose foams can be assured, direct measurement of the wettability of molten PCMs on the surface of supporting materials is interesting if their quick solidification could be resolved [29].

The effect of the chemical modifications of CNF foams on their PCM-stabilization was tested (Fig. 3). One thing to mention is that it is more reliable to evaluate the PCM leakage situation by weighing the mass of the leaked PCM, especially when the leakage areas of PCM samples do not differ much. For composite PCMs supported by pristine CNF foams, more leaked Pw rather than PEG was visible on the filter paper, and the leakage percentage of Pw is

higher than that of PEG (Tables 2 & 3), which suggests the importance of the affinity between supporting materials and PCMs for a stable form. When CNF_{APTMS} foams were used to encapsulate PCMs, it was found that PEG-based composite PCM exhibited less leakage while Pw-based composite PCM exhibited more leakage, also evidenced by the results in Tables 2 & 3. Analogously, CNF_{MTMS} foams provided a greater stabilization effect to Pw, and less PCM leakage was seen. In contrast, these hydrophobic foams imparted an inferior stabilization effect on PEG, and PCM leakage increased accordingly. These results prove the importance of tuning the surface chemistry of supporting materials on the shape-stability of PCMs, which significantly affects their actual applications. Therefore, CNF_{APTMS} foams and CNF_{MTMS} foams were used to fabricate PEG-based composite PCMs and Pw-based composite PCMs, respectively.

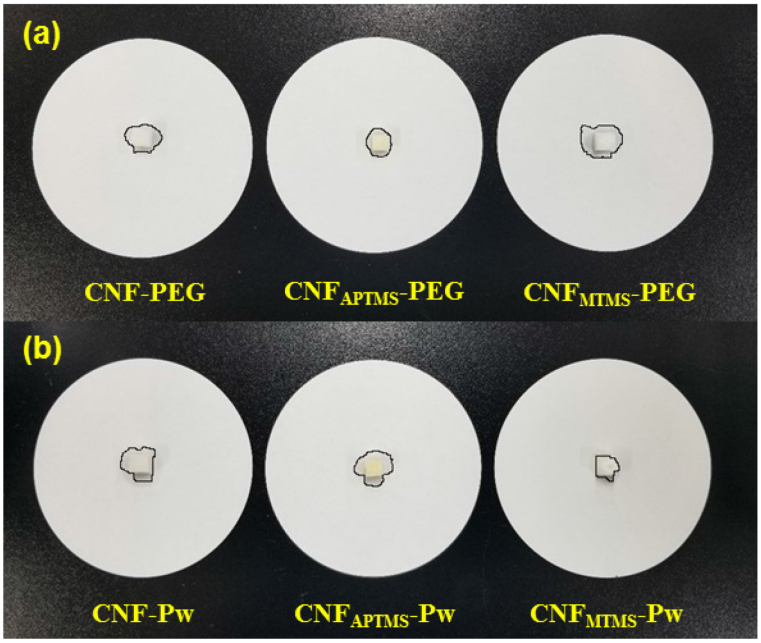

Fig. 3. Effect of the chemical modifications of CNF foams on their PCM-stabilization effect: leakage testing of (a) PEG-based composite PCMs and (b) Pw-based composite PCMs.

Table 2. PEG leakage percentage of different foam-stabilized composite PCMs.

Composite PCM	Weight before test (g)	Weight after test (g)	Weight of the leaked PEG (g)	Leakage percentage (%)
CNF-PEG	0.675	0.662	0.013	1.93
CNF_{APTMS}-PEG	0.47	0.462	0.008	1.70
CNF_{MTMS}-PEG	0.489	0.472	0.017	3.48

Table 3. Pw leakage percentage of different foam-stabilized composite PCMs.

Composite PCM	Weight before test (g)	Weight after test (g)	Weight of the leaked Pw (g)	Leakage percentage (%)
CNF-Pw	0.474	0.464	0.01	2.11
CNF_{APTMS}-Pw	0.431	0.419	0.012	2.78
CNF_{MTMS}-Pw	0.568	0.563	0.005	0.88

3.2 Morphologies and structures of composite PCMs

The morphologies and structures of the prepared composite PCMs, supporting foams and related starting materials CNF and CNT are presented in Fig. 4. Fig.4a shows the typical morphology of CNF, i.e., dozens of nanometers in diameter and several micrometers in length, and the high aspect ratio of CNF benefit the entanglement of the adjacent nanofibrils, which is also visible in the TEM image. In the present work, CNTs were used as the heat transfer enhancers for the prepared composite PCMs, and the morphology of an individual CNT is shown in Fig. 4b. As noticed, CNT has a comparable diameter with CNF but is short in length. Figs 4c and 4d present the porous structure of the prepared CNF-based foams, and these nanocellulose-based foams exhibit lamellar architectures and open porosity, as reported elsewhere [30]. The presented foams displayed irregular arrangements of thin plates in the form of films or nanopapers that are connected by partially fibrillated fibers or dangling mass. In particular, the porous structures of such foams can be easily controlled by the concentration of CNF suspensions for foam preparation and processing parameters such as the freezing rate and freezing direction of CNF suspensions [31,32]. In this work, the concentration of starting CNF suspensions was fixed at 2% based on our previous results [31], and silylation reaction and CNT introduction were performed in these suspensions, followed by liquid nitrogen freezing and freeze drying.

With the increased introduction of CNTs, the foams became denser, and their porosities decreased accordingly (Tables 4 and S1). The possible reason is that CNTs attached to the CNF surface, and the foam voids were partially filled with CNTs. Fig. S3 shows the distribution of CNTs in the CNF-based foam skeleton, and they are found to be uniformly located in the observed areas and partially filled the pores in the foams, which led to decreased PCM absorption capacity but greater PCM stabilization (Table S1).

Figs. 4e and 4f present the internal structure of composite PCMs that were prepared by impregnating the porous foams with the molten PCMs. No holes or voids exist in the two composites, which indicates favorable PCM absorption into the porous structures of the two chemically modified CNF-based porous scaffolds. Given the low density and high porosity of the two porous scaffolds (Table 4), the obtained PCM composites exhibit high loading factions of PCMs (i.e. 93.63% of PEG and 91.77% of Pw), which contributes to high phase change enthalpy for practical uses. Moreover, no evident interfaces between the components are noticed. Such features indicate good compatibility between the components [33], which was mainly contributed by the chemistry tuning of CNF-based scaffolds.

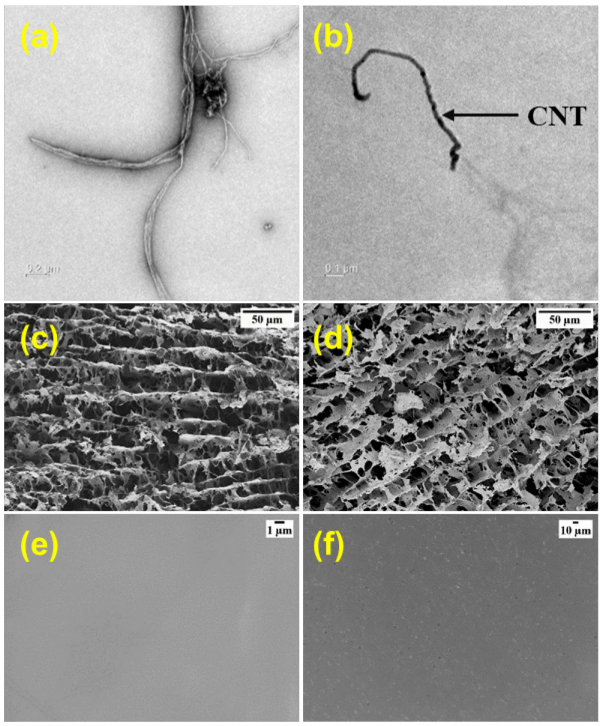

Fig. 4. TEM images of (a) CNF and (b) CNT; SEM images of (c) CNF_{APTMS}/CNT_{50} foam, (d) CNF_{MTMS}/CNT_{50} foam, (e) CNF_{APTMS}/CNT_{50}-PEG composite and (f) CNF_{MTMS}/CNT_{50}-Pw composite.

The leakage testing of the prepared composite PCMs was conducted to confirm their form-stability, and the results are shown in Fig. 5 and Table 4. For the CNF_{APTMS}/CNT_{50}-PEG composite, the PCM leakage percentage was 1.81%, which is slightly higher than that of the CNF_{APTMS}-PEG composite. The possible reason is that the introduction of CNTs may interfere

with the internal structure of foams and thus the absorption and stabilization of PCMs. Similarly, the CNF_{MTMS}/CNT_{50}-Pw composite also exhibits slightly higher PCM leakage than CNF_{MTMS}-Pw composite. Despite so, the as-prepared CNF_{APTMS}/CNT_{50}-PEG composite has PCM fraction of 93.63%, and CNF_{MTMS}/CNT_{50}-Pw composite has a PCM fraction of 91.77%, a value higher than previously reported results (40–50% [34], 40–70% [35], 77.5% [36], 85% [6], 70–90% [37]). Composite PCMs with high loading levels of PCM are preferred for practical uses due to their high energy storage density and cost-effectiveness. Meanwhile, the negligible PCM leakage of the obtained composite PCMs favors their long-term energy storage applications

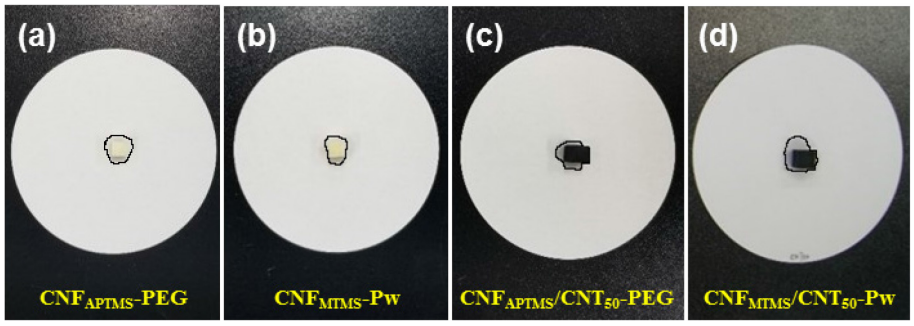

Fig. 5. Leakage testing of foam-stabilized composite PCMs on filter paper: (a) CNF_{APTMS}-PEG, (b) CNF_{MTMS}-Pw, (c) CNF_{APTMS}/CNT_{50}-PEG and (d) CNF_{MTMS}/CNT_{50}-Pw.

Table 4. The effect of CNF-based foams on the PCM absorption capacity and leakage percentage.

Foam	Foam density (kg/m^3)	Foam porosity (%)	PCM absorption capacity (%)	PCM Leakage percentage (%)
CNF_{APTMS}	59.88	94.78	94.40	1.70
CNF_{APTMS}/CNT_{50}	67.26	94.52	93.63	1.81
CNF_{MTMS}	59.91	96.57	92.08	0.88
CNF_{MTMS}/CNT_{50}	64.53	96.39	91.77	1.71

3.3 Chemical and crystalline structure analyses

The chemical structures of composite PCMs and their components were examined by FT-IR, and the collected spectra are presented in Figs. 6a and b. As shown in Fig. 6a, the spectrum of neat CNF exhibits absorption bands at 3328 cm^{-1} and 897 cm^{-1} that are ascribed to the hydroxyls groups and characteristic glucosidic linkages of cellulose structures, respectively

[38]; the spectrum of APTMS modified CNF (i.e. CNF_{APTMS}) displayed new banks at 1610, 1506, 1226, 1032, and 694 cm^{-1} that can be assigned to $-NH_2$ in-plane deformation, $-CH_2-$ scissoring, Si–C bending, Si–O stretching, and $-NH_2$ out-of-plane bending vibrations, respectively [39]; the spectrum of MTMS modified CNF (i.e. CNF_{MTMS}) displayed a characteristic broad band at 897 cm^{-1} that is assigned to Si–OH stretching, and a sharp band at 777 cm^{-1} that is ascribed to Si–C and/or Si–O stretching [40]. These changes in FT-IR spectra suggest the successful chemical modification of CNF. The FT-IR spectra of PEG and Pw are displayed in Fig. 6b. In the FT-IR spectrum of pristine PEG, characteristics peak at 3342 cm^{-1} ascribed to the stretching vibration of O−H group and 1107 cm^{-1} due to the C−O−C symmetric stretching vibration, peaks at 2887 cm^{-1}, 1469 cm^{-1}, 949 cm^{-1} and 841 cm^{-1} corresponding to the C−H vibration [41], are visible. In the spectrum of Pw, bands at 2916 cm^{-1} and 2848 cm^{-1} are ascribed to C−H stretching of $-CH_3$ and $-CH_2$ groups, respectively, which are the characteristics of alkanes [42]. The spectra of the prepared CNF_{APTMS}/CNT_{50}-PEG and CNF_{MTMS}/CNT_{50}-Pw composite PCMs are found to be simply the mixture of the characteristic peaks of corresponding porous scaffolds (i.e., CNF/CNT foams) and PCMs, and no extra peaks were generated (Fig. 6b), indicating the absence of chemical reactions between the scaffolds and PCMs. Therefore, PCM was encapsulated in the porous foam via physical absorption.

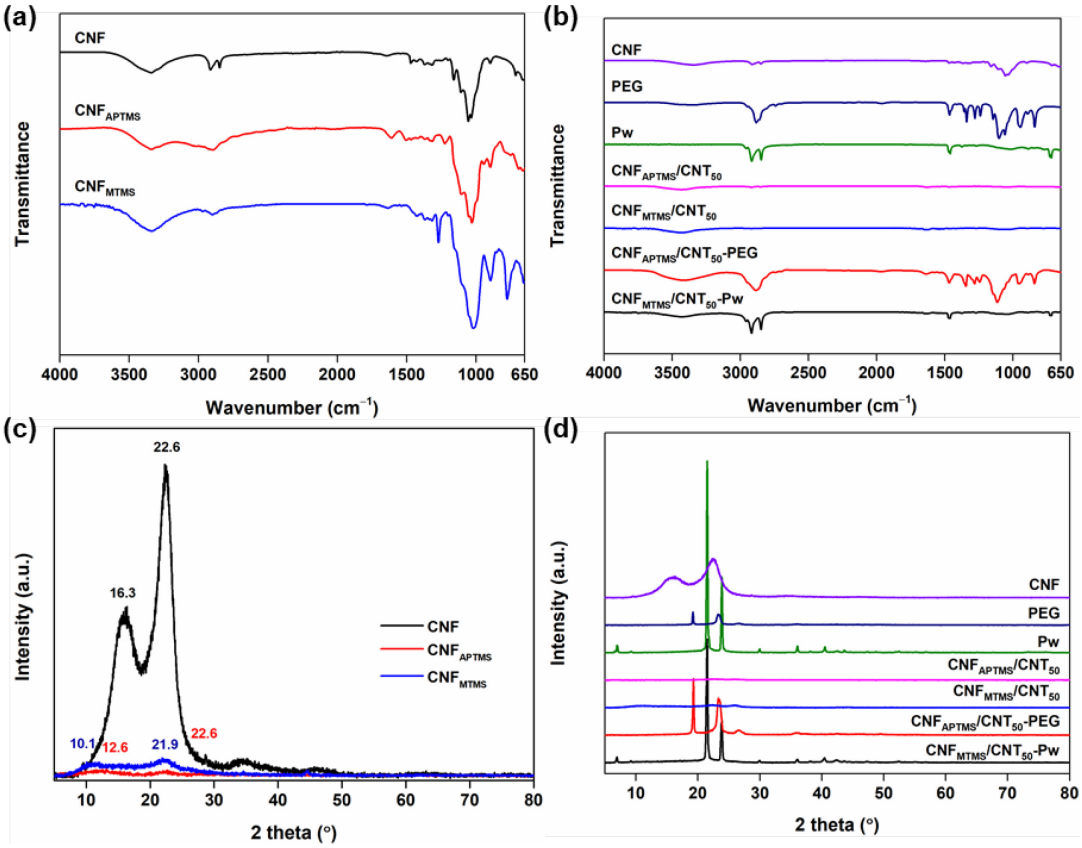

Fig. 6. FT-IR spectra of (a) pristine CNF and chemically modified CNF, and (b) composite PCMs and related components; XRD patterns of (c) pristine CNF and chemically modified CNF, and (d) composite PCMs and related components.

The crystalline structures of composite PCMs and their components were investigated, and the obtained XRD patterns are shown in Figs. 6c and 6d. The XRD pattern of pristine CNF shows the characteristic peaks at 16.2° and 22.2° that are assigned to the (110) and (200) crystal planes of cellulose, respectively (Fig. 6c) [43]. The XRD pattern of silylated CNF (i.e., CNF_{APTMS} and CNT_{MTMS}) differed from the XRD pattern of pristine CNF, i.e., the peak at 16.3° shifted to left, which is assigned to the conversions of polymorphs from the original cellulose I to cellulose II and indicates the success of chemical modification of CNF [44]. Fig. 6d compares the XRD patterns of neat PCM and the prepared composite PCMs. It was found that the patterns of composite PCMs show two main diffraction peaks similar to those of neat PCMs, indicating that using CNF-based hybrid foam to encapsulate PCMs did not affect their crystal structure [45]. Similar to the FT-IR results, the diffraction peaks of the composite PCMs contain all the characteristic peaks from their corresponding components, and no new peaks appear. This again,

verified the absence of chemical reactions or interactions between the supporting scaffolds and PCMs.

3.4 Phase change and thermal properties

Thermal energy storage and release by PCMs are fulfilled through their phase transitions, and the thermal properties of PCMs such as thermal conduction performance and thermal stability are critical to the speed and efficiency of energy storage. Therefore, it is necessary to examine the phase change and thermal properties of the prepared composite PCMs. The phase change enthalpies and transition temperature of PCM samples were determined by DSC method. As illustrated by Fig. 7a, all DSC curves of PEG-based PCM samples displayed one main phase change peak during both melting (endothermic) and freezing (exothermic) processes, which corresponds to the solid-liquid phase transitions. However, the DSC curves of Pw-based PCM samples exhibited two peaks during their phase transitions (Fig. 7b). The lower-temperature peak was assigned to the solid–solid phase transition, and the higher-temperature peak was attributed to the solid–liquid phase transition [46]. The phase change enthalpies and transition temperature of PCM samples are extracted from the DSC curves and are listed in Tables 5 and 6. The phase change enthalpy of neat PEG is 151.1 kJ/kg, and the melting temperature, onset temperature, is 26.1 °C during heating, and similar values were obtained during cooling. As noticed, neat PEG exhibits quite close melting temperature and freezing temperature, indicating the absence of supercooling problem, which is an advantage of organic PCMs. The phase change temperatures of composite PCMs are slightly lower than that of neat PEG, which can be attributed to the improved form-stability that enhances the heat transfer efficiency in phase transitions [47]. The phase change enthalpies of the prepared composite PCMs are 4.6%–5.4% lower than the enthalpy of neat PEG because non-phase change components (i.e., CNF and CNTs) were incorporated. These enthalpy reductions roughly agree with the PEG fractions of the prepared composite PCMs (Table S1). Similar findings can also be extracted for Pw-based PCM samples, i.e., reason phase change temperatures and enthalpies were obtained. Besides, composite PCMs prepared in this work exhibit relatively higher enthalpies than the composites reported elsewhere [46,48–52]. The high loading levels of PCMs and the superior form-stability

of the composite PCMs would contribute to their favorable phase change performance for practical applications.

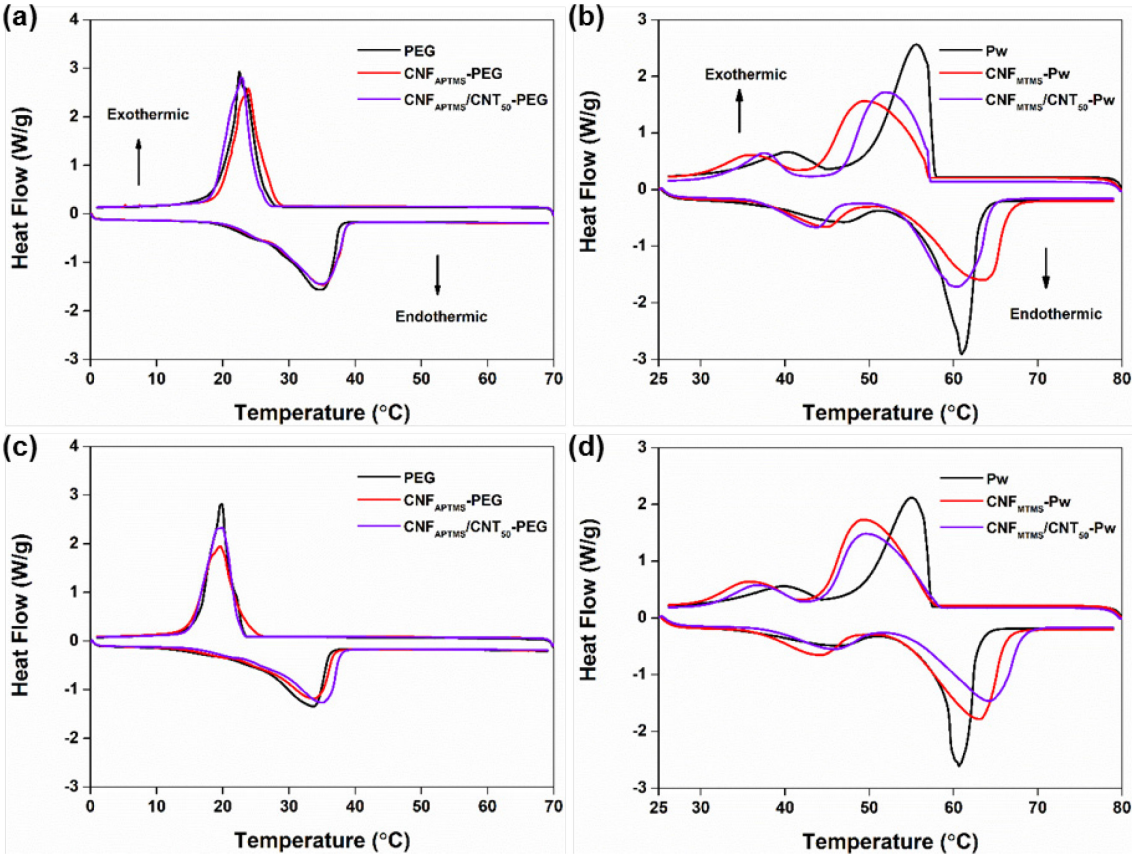

Fig. 7. DSC curves of (a) PEG and PEG-based composite PCMs and (c) their curves after 100 cycles of melting and freezing; (b) Pw and Pw-based composite PCMs and (d) their curves after 100 cycles of melting and freezing.

Table 5. Melting points, freezing points and enthalpies of PEG-based PCM samples.

PCM sample	Heating process			Cooling process		
	Melting point (°C)	Enthalpy (kJ/kg)	Enthalpy reduction (%)	Freezing point (°C)	Enthalpy (kJ/kg)	Enthalpy reduction (%)
PEG	26.1	151.4	–	26.2	151.3	–
CNF_{APTMS}-PEG	25.2	144.2	4.76	25.6	144.3	4.63
CNF_{APTMS}/CNT_{50}-PEG	25.2	143.3	5.35	24.9	143.1	5.42

Table 6. Melting points, freezing points and enthalpies of Pw-based PCM samples.

PCM sample	Heating process			Cooling process		
	Melting point (°C)	Enthalpy (kJ/kg)	Enthalpy reduction (%)	Freezing point (°C)	Enthalpy (kJ/kg)	Enthalpy reduction (%)
Pw	57.7	202.8	-	55.5	202.7	-
CNF_{MTMS}-Pw	54.2	185.9	8.3	57.0	185.9	8.3
CNF_{MTMS}/CNT_{50}-Pw	53.4	184.6	9.0	57.2	184.5	9.0

Thermal reliability of PCMs is desired for their reliable and durable applications. The thermal reliabilities of the prepared composite PCMs were determined by measuring their phase change properties after a number of thermal cycles. The phase change enthalpies and transition temperatures of the prepared composite PCMs after 100 melting/freezing cycles that are extracted from DSC curves (Figs. 7c and 7d) are summarized in Tables S2 and S3. Results show that the phase change enthalpies of PEG-based composite PCMs decreased approximately by 12%–14%, while the Pw-based composite PCMs decreased approximately by 2%–6%, indicating their unfavorable thermal reliability for long-term applications. Unexpectedly, the phase change enthalpies of neat PEG and Pw also decreased after 100 thermal cycles. This is possibly related to their relatively low molecular weight, which may cause the potential degradation of PCM in repeated heating and cooling. Despite so, the thermal reliability of the prepared composite PCMs should be improved in future work.

Thermal stabilities of neat PCM and the prepared composite PCMs were evaluated by thermogravimetric analysis (Fig. 8). As shown in Fig. 8a, the weight loss of neat PEG began at 220 °C, 50 wt% of this sample decomposed at 372.6 °C, and its decomposition completed at 420 °C, and the residual mass of neat PEG after heating approaches zero, and similar thermal degradation process was reported elsewhere [50,53]. Compared to neat PEG, the prepared composite PCMs exhibited slower rates of weight loss during heating, i.e., 50 wt% of CNF_{APTMS}-PEG decomposed at 393.4 °C, and 50 wt% of CNF_{APTMS}/CNT_{50}-PEG decomposed at 404 °C; and their weight losses completed at higher temperatures (approximately 425 °C for CNF_{APTMS}-PEG and 435 °C for CNF_{APTMS}/CNT_{50}-PEG), indicating their improved thermal

stabilities. The residual mass of composite PCMs is higher than that of neat PEG, which can be correlated to the introduction of thermal stable ingredient CNTs that are even stable at temperatures up to approximately 800 °C [54]. In particular, CNFs used in this work were prepared from bleached kraft pulp where the amounts of hemicellulose and lignin can be ignored. Considering that cellulose has a pyrolysis temperature of 315–400 °C [55], it may also positively contribute to the improved thermal stability of composite PCMs under heating. It is reasonable that the final residual solid content of CNF_{APTMS}/CNT_{50}-PEG was the highest among all the tested PCM samples because of its higher addition levels of thermally stable CNTs. Similar findings can also be seen for Pw-based composite PCMs (Fig. 8b), i.e., the decomposition temperature of composite PCMs (approximately 350 °C) are higher than that of neat Pw (315 °C) and more residues retained for composite PCMs due to the incorporation of relatively stable foam scaffolds. In conclusion, the prepared composite PCMs exhibit greater thermal stabilities over neat PCMs, which is likely to benefit their high-temperature applications.

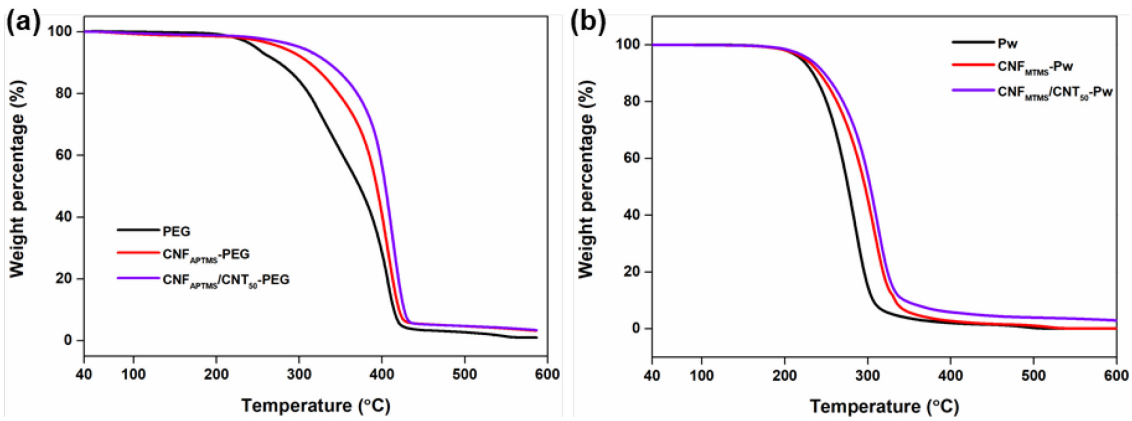

Fig. 8. Thermogravimetric curves of (a) PEG and PEG-based composite PCMs and (b) Pw and Pw- based Composite PCMs.

3.5 Application investigation of composite PCMs

Solar energy harvesting and utilization is one of the most promising application scenarios for PCMs. To investigate the heat absorption behavior of PCM samples under sunlight, Xenon lamp with a full solar spectrum was used as the heat source, and the real-time temperature of

samples was recorded (Figs. 9a & 9b). The neat PCM samples were not tested because of their rapid melting and serious leakage during heating. On the contrary, the tested composite samples remained almost intact upon heating, which indicated their favorable form-stabilities. During the whole heating process, the temperature of composite PCMs without CNTs is always lower than that of composite PCMs containing CNTs. Moreover, a higher CNT content led to faster temperature rise and higher final temperature before removing the heat source. These findings are consistent with those in other reports [56–58]. After removing the lamp, the PCM samples started to release the stored energy, after which the sample temperature gradually decreased to ambient level. It was found that the heat release period of composite PCMs containing CNTs is longer than that of neat PCMs and composite PCMs without CNTs, indicating that the former samples absorbed and stored more latent heat during heating. Interestingly, the final temperatures of all samples decreased to ambient temperature almost simultaneously, which suggests that composite PCMs containing CNTs experienced more quick heat transfer from samples to the surroundings. These observations verified the enhanced thermal conduction performance of composite PCMs containing CNTs, which may contribute to more efficient heat storage applications.

The measure thermal conductivities of PCM samples are presented in Fig. 9c. The results indicate that CNT-containing PCM composites exhibited improved thermal conductivity over pure PCM, which can be attributed to the excellent heat transfer performance of CNTs. The thermal conductivity of CNF_{APTMS}/CNT_{50}-PEG and CNF_{MTMS}/CNT_{50}-Pw is 15.1% and 13.9% higher than that of neat PEG and Pw, respectively. These results along with the results in Figs. 8a and b proved that the introduction of CNTs improved the heat transfer performance of PCM composites. Nevertheless, one thing to confess is that the improvement in thermal conductivities of PCMs is not sufficiently high. Two reasons may account for the low absolute values of the thermal conductivity of CNF_{APTMS}/CNT_{50}-PEG and CNF_{MTMS}/CNT_{50}-Pw. First of all, the high PCM fractions (93.63% for PEG and 91.77% for Pw) in the PCM composites suppressed the improvement in thermal conductivity [59]. Secondly, thermal conductive properties along the CNT axis are very different from the transverse direction (estimated up to 3500 W/(m•K) in the axial direction vs. 10.23 W/(m•K) in the transverse direction [60]), thus

the anisotropic distribution of hollow CNTs in PCM composites directly affected the thermal conductivity values. Similar observations have been reported elsewhere [59]. Therefore, the type and dose of carbon nanomaterials should be care for when they are used to enhance the thermal conductivity of PCMs.

It is known that TEG is a type of solid-state semiconductor device that converts a temperature difference and heat flow into a useful DC power source, and PCMs-based heat exchangers can be applied to transfer and dissipate heat for the optimization of the thermal management system of TEGs [61]. Novel PCM sandwich structures (Fig. 1.) were designed for actual application based on the differences between the phase change performances of PEG and Pw. Pw-based composite PCM with high CNT content (i.e. CNF_{MTMS}/CNT_{50}-Pw) was placed on the top of TEG due to its high phase change enthalpy (184.6 kJ/kg) and relatively high phase transition temperature (53.4 ºC); PEG-based composite PCMs were attached to the bottom of TEG because of its lower phase transition temperature (about 25 ºC). A thermoelectric generator is positioned in the middle of two pieces of composite PCMs for voltage generation. Due to such a structure design, the original heat sink that is attached to the bottom of TEG for better heat dissipation was replaced by the PEG-based composite PCM. As shown in Fig. 9d, the control (i.e., TEG without any PCMs on it) generated a 0.05 V voltage during heating, a value approximately half of that in Fig. S4. The reason might be that the original aluminum heat sink structure was immersed in iced water, and this gave a faster heat dissipation to the TEG bottom surface and then a greater temperature difference between TEG top and bottom surfaces, which resulted in more efficient voltage generation [62]. When only CNF_{MTMS}/CNT_{50}-Pw was positioned on the top surface of TEG, the generated voltage gradually increased and then leveled off at 0.10 V during sunlight irradiation. A similar tendency was observed when PCM sandwich structure I was applied, and the higher voltage of 0.14 V can be ascribed to the improved heat absorption and dissipation of the TEG bottom surface contributed by CNT_{APTMS}-PEG composite PCM. When PCM sandwich structure II was applied, the maximum voltage level was unaffected, but two voltage plateau regions appeared. The occurrence of steady voltage generation can be attributed to the phase transitions of composite PCMs that create stable temperature differences of TEG surfaces. When the sunlight irradiator was removed, all

the curves showed slower voltage decline than did the control, which can be attributed to the decrease of temperature difference of two TEG surfaces by the released heat from composite PCMs, as evidenced by the curves at the time length of 4000–5500 s. Therefore, the proposed PCM sandwich structures exhibit attractive heat absorption and dissipation, and more efficient voltage maintenance in the absence of heating power was observed. However, the voltage level should be improved when using these PCM sandwich structures for practical applications such as solar-thermal-electricity conversion systems, and this will be the focus of our future work.

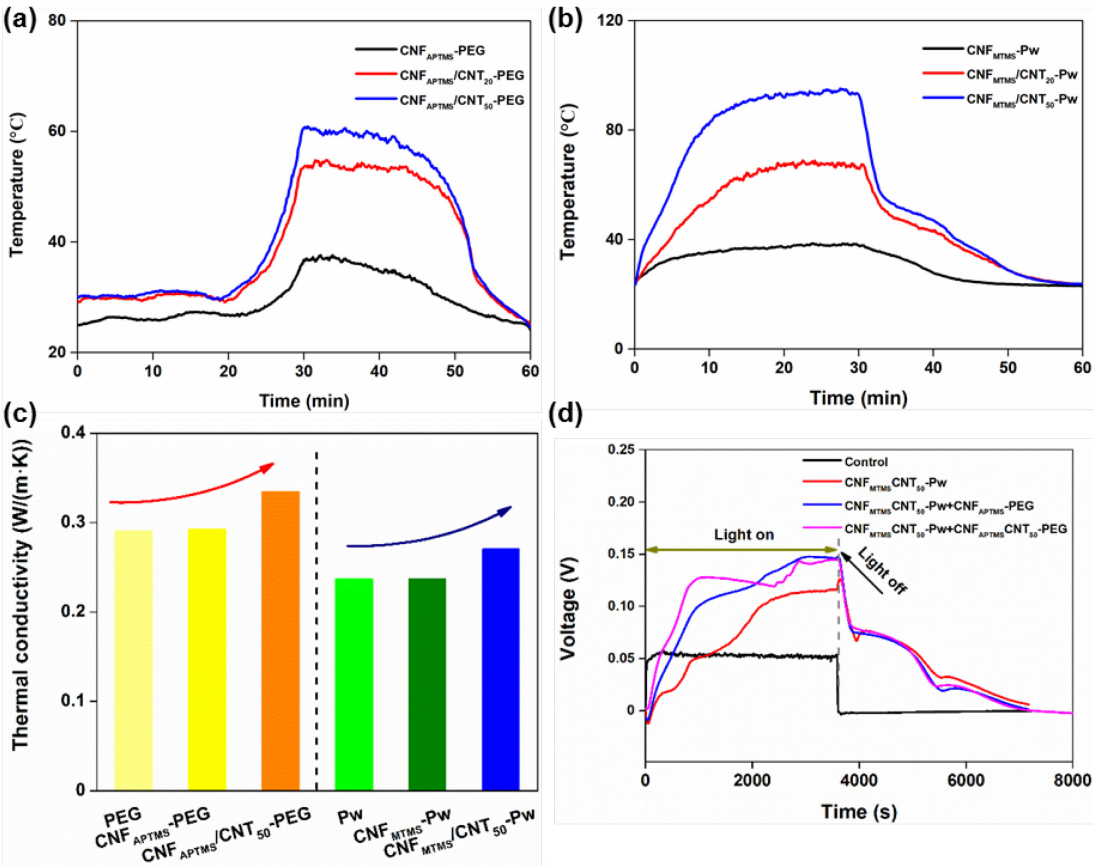

Fig. 9. Temperature- heating time curves of (a) PEG based Composite PCMs and (b) Pw based PCM under solar simulator, (c) thermal conductivity of PCM samples and (d) time course of the open-circuit voltage of the thermoelectric generator with/without sandwich PCMs on it.

4. Conclusion

The present study suggests the importance of surface chemistry tuning and thermal conductivity enhancer introduction of supporting scaffolds for the performance improvement of organic PCMs. Chemistry modification of CNF enhanced the foam shape-stability and its affinity with PCMs. The prepared composite PCMs had compact structures with high loading levels of PCMs (93.63% for PEG and 91.77% for Pw) due to the highly porous foam structure and favorable foam-PCM compatibility. Meanwhile, the use of CNF-based foams remarkably inhibited PCM leakage during their phase transitions. Consequently, the prepared composite PCMs exhibited reasonable phase change enthalpies and phase transition temperatures. Due to the introduction of CNTs, composite PCMs displayed enhanced thermal stability and heat conduction performance, which benefit their applications in solar energy harvesting, storage and utilization because of the enhanced sunlight absorption and heat transfer. Interestingly, the designed PCM sandwich structure in this research is also promising for voltage maintenance of TEG-based power systems in the lack of sunlight irradiation. Nevertheless, the thermal conductivity and thermal reliability of composite PCMs needs to be further improved for long-term LHS applications. Overall, the present work shows the potential of sustainable polymer-based supporting scaffolds for the preparation and energy application of form-stable composite PCMs.

■ Associated Content

See supplementary data.

CRediT authorship contribution statement

Zhenghui Shen and Soojin Kwon contributed equally to this work. **Zhenghui Shen**: Conceptualization, Methodology, Investigation, Writing-Original Draft. **Soojin Kwon**: Conceptualization, Methodology, Investigation, Writing-Original Draft. **Hak Lae Lee**: Writing-Review & Editing, Supervision. **Martti Toivakka**: Writing-Review & Editing. **Kyudeok Oh**: Conceptualization, Methodology, Investigation, Writing-Review & Editing, Funding acquisition.

Declaration of Competing Interest

The authors declare that they have no known competing financial interests or personal relationships that could have appeared to influence the work reported in this paper.

Acknowledgments

This work was supported by research fund of Chungnam National University. Professor Hye Jung Youn is thanked for her assistance in preparing CNF.

References

[1] W. Aftab, A. Usman, J. Shi, K. Yuan, M. Qin, R. Zou, Phase change material-integrated latent heat storage systems for sustainable energy solutions, Energy Environ. Sci. 14 (8) (2021) 4268–4291. https://doi.org/10.1039/D1EE00527H.

[2] S.A. Mohamed, F.A. Al-Sulaiman, N.I. Ibrahim, Md.H. Zahir, A. Al-Ahmed, R. Saidur, B.S. Yılbaş, A.Z. Sahin, A review on current status and challenges of inorganic phase change materials for thermal energy storage systems, Renew. Sust. Energ. Rev. 70 (2017) 1072–1089. https://doi.org/10.1016/j.rser.2016.12.012.

[3] M.M. Farid, A.M. Khudhair, S.A.K. Razack, S. Al-Hallaj, A review on phase change energy storage: materials and applications, Energy Convers. Manag. 45(9–10) (2004) 1597–1615. https://doi.org/10.1016/j.enconman.2003.09.015.

[4] A. Safari, R. Saidur, F.A. Sulaiman, Y. Xu, J. Dong, A review on supercooling of phase change materials in thermal energy storage systems, Renew. Sust. Energ. Rev. 70 (2017) 905–919. https://doi.org/10.1016/j.rser.2016.11.272.

[5] D.G. Atinafu, Y.S. Ok, H.W. Kua, S. Kim, Thermal properties of composite organic phase change materials (PCMs): A critical review on their engineering chemistry, Appl. Therm. Eng. 181 (2020) 115960. https://doi.org/10.1016/j.applthermaleng.2020.115960.

[6] M.R. Yazdani, R. Ajdary, A. Kankkunen, O.J. Rojas, A. Seppälä, Cellulose nanofibrils endow phase-change polyethylene glycol with form control and solid-to-gel transition for thermal energy storage, ACS Appl. Mater. Interfaces. 13 (5) (2021) 6188–6200. https://doi.org/10.1021/acsami.0c18623.

[7] Y. Zhao, L. Jin, B. Zou, G. Qiao, T. Zhang, L. Cong, F. Jiang, C. Li, Y. Huang, Y. Ding, Expanded graphite-paraffin composite phase change materials: Effect of particle size on the composite structure and properties, Appl. Therm. Eng. 171 (2020) 115015. https://doi.org/10.1016/j.applthermaleng.2020.115015.

[8] L. Liu, J. Chen, Y. Qu, T. Xu, H. Wu, G. Huang, X. Zhou, L. Yang, A foamed cement blocks with paraffin/expanded graphite composite phase change solar thermal absorption material, Sol. Energy Mater Sol. Cells. 200 (2019) 110038. https://doi.org/10.1016/j.solmat.2019.110038.

[9] S. Sundararajan, A.B. Samui, P.S. Kulkarni, Versatility of polyethylene glycol (PEG) in designing solid-solid phase change materials (PCMs) for thermal management and their application to innovative technologies, J. Mater. Chem. A. 5 (35) (2017) 18379–18396. https://doi.org/10.1039/C7TA04968D.

[10] S. Ramakrishnan, J. Sanjayan, X. Wang, M. Alam, J. Wilson, A novel paraffin/expanded perlite composite phase change material for prevention of PCM leakage in cementitious composites, Appl. Energy. 157 (2015) 85–94. https://doi.org/10.1016/j.apenergy.2015.08.019.

[11] K. Yu, Y. Liu, Y. Yang, Review on form-stable inorganic hydrated salt phase change materials: Preparation, characterization and effect on the thermophysical properties, Appl. Energy. 292 (2021) 116845. https://doi.org/10.1016/j.apenergy.2021.116845.

[12] D. Klemm, B. Heublein, H.-P. Fink, A. Bohn, Cellulose: Fascinating biopolymer and sustainable raw material, Angew. Chem. Int. Ed. 44 (22) (2005) 3358–3393. https://doi.org/10.1002/anie.200460587.

[13] D. Klemm, F. Kramer, S. Moritz, T. Lindström, M. Ankerfors, D. Gray, A. Dorris, Nanocelluloses: A new family of nature-based materials, Angew. Chem. Int. Ed. 50 (24) (2011) 5438–5466. https://doi.org/10.1002/anie.201001273.

[14] S. Ummartyotin, H. Manuspiya, A critical review on cellulose: From fundamental to an approach on sensor technology, Renewable and Sustainable Energy Reviews. 41 (2015) 402–412. https://doi.org/10.1016/j.rser.2014.08.050.

[15] H. Lee, J. Sundaram, S. Mani, Production of cellulose nanofibrils and their application to

652 food: A review, In: R. Prasad, V. Kumar, M. Kumar (Eds.), Nanotechnology, Springer
653 Singapore, Singapore, 2017: pp. 1–33. https://doi.org/10.1007/978-981-10-4678-0_1.
654 [16] M. Pääkkö, M. Ankerfors, H. Kosonen, A. Nykänen, S. Ahola, M. Österberg, J.
655 Ruokolainen, J. Laine, P.T. Larsson, O. Ikkala, T. Lindström, Enzymatic hydrolysis
656 combined with mechanical shearing and high-pressure homogenization for nanoscale
657 cellulose fibrils and strong gels, Biomacromolecules. 8 (6) (2007) 1934–1941.
658 https://doi.org/10.1021/bm061215p.
659 [17] Q.-F. Guan, H.-B. Yang, Z.-M. Han, L.-C. Zhou, Y.-B. Zhu, Z.-C. Ling, H.-B. Jiang, P.-F.
660 Wang, T. Ma, H.-A. Wu, S.-H. Yu, Lightweight, tough, and sustainable cellulose
661 nanofiber-derived bulk structural materials with low thermal expansion coefficient, Sci.
662 Adv. 6 (18) (2020) eaaz1114. https://doi.org/10.1126/sciadv.aaz1114.
663 [18] X. Chen, P. Cheng, Z. Tang, X. Xu, H. Gao, G. Wang, Carbon-based composite phase
664 change materials for thermal energy storage, transfer, and conversion, Adv. Sci. 8 (9)
665 (2021) 2001274. https://doi.org/10.1002/advs.202001274.
666 [19] K. Yuan, J. Shi, W. Aftab, M. Qin, A. Usman, F. Zhou, Y. Lv, S. Gao, R. Zou, Engineering
667 the thermal conductivity of functional phase-change materials for heat energy conversion,
668 storage, and utilization, Adv. Funct. Mater. 30 (8) (2020) 1904228.
669 https://doi.org/10.1002/adfm.201904228.
670 [20] S. Wu, T. Yan, Z. Kuai, W. Pan, Thermal conductivity enhancement on phase change
671 materials for thermal energy storage: A review, Energy Stor. Mater. 25 (2020) 251–295.
672 https://doi.org/10.1016/j.ensm.2019.10.010.
673 [21] J.N. Coleman, U. Khan, W.J. Blau, Y.K. Gun'ko, Small but strong: A review of the
674 mechanical properties of carbon nanotube-polymer composites, Carbon. 44 (9) (2006)
675 1624–1652. https://doi.org/10.1016/j.carbon.2006.02.038.
676 [22] W. Yang, Z. Zhao, K. Wu, R. Huang, T. Liu, H. Jiang, F. Chen, Q. Fu, Ultrathin flexible
677 reduced graphene oxide/cellulose nanofiber composite films with strongly anisotropic
678 thermal conductivity and efficient electromagnetic interference shielding, J. Mater. Chem.
679 C. 5 (15) (2017) 3748–3756. https://doi.org/10.1039/C7TC00400A.
680 [23] Y. Li, H. Zhu, F. Shen, J. Wan, S. Lacey, Z. Fang, H. Dai, L. Hu, Nanocellulose as green

dispersant for two-dimensional energy materials, Nano Energy. 13 (2015) 346–354. https://doi.org/10.1016/j.nanoen.2015.02.015.

[24] Q. Zheng, Z. Cai, S. Gong, Green synthesis of polyvinyl alcohol (PVA)-cellulose nanofibril (CNF) hybrid aerogels and their use as superabsorbents, J. Mater. Chem. A. 2 (9) (2014) 3110–3118. https://doi.org/10.1039/C3TA14642A.

[25] S. Jiang, M. Zhang, M. Li, L. Liu, L. Liu, J. Yu, Cellulose nanofibril (CNF) based aerogels prepared by a facile process and the investigation of thermal insulation performance, Cellulose. 27 (11) (2020) 6217–6233. https://doi.org/10.1007/s10570-020-03224-4.

[26] Z.A. Qureshi, H.M. Ali, S. Khushnood, Recent advances on thermal conductivity enhancement of phase change materials for energy storage system: A review. Int. J. Heat Mass Transf. 127 (2018) 838–856. https://doi.org/10.1016/j.ijheatmasstransfer.2018.08.049.

[27] K. Khwaldia, E. Arab-Tehrany, S. Desobry, Biopolymer coatings on paper packaging materials, Compr. Rev. Food Sci. Food Saf. 9 (1) (2010) 82–91. https://doi.org/10.1111/j.1541-4337.2009.00095.x.

[28] J.-W. Rhim, Effect of moisture content on tensile properties of paper-based food packaging materials, Food Sci. Biotechnol. 19 (1) (2010) 243–247. https://doi.org/10.1007/s10068-010-0034-x.

[29] S. Wu, T. Li, Z. Tong, J. Chao, T. Zhai, J. Xu, T. Yan, M. Wu, Z. Xu, H. Bao, T. Deng, R. Wang, High-performance thermally conductive phase change composites by large-size oriented graphite sheets for scalable thermal energy harvesting. Adv. Mater. 31 () (2019) 1905099. https://doi.org/10.1002/adma.201905099.

[30] F. Martoïa, T. Cochereau, P.J.J. Dumont, L. Orgéas, M. Terrien, M.N. Belgacem, Cellulose nanofibril foams: Links between ice-templating conditions, microstructures and mechanical properties, Mater. Des. 104 (2016) 376–391. https://doi.org/10.1016/j.matdes.2016.04.088.

[31] Z. Shen, S. Kwon, H.L. Lee, M. Toivakka, K. Oh, Cellulose nanofibril/carbon nanotube composite foam-stabilized paraffin phase change material for thermal energy storage and conversion, Carbohydr. Polym. 273 (2021) 118585.

https://doi.org/10.1016/j.carbpol.2021.118585.

[32] K. Kriechbaum, P. Munier, V. Apostolopoulou-Kalkavoura, N. Lavoine, Analysis of the porous architecture and properties of anisotropic nanocellulose foams: A novel approach to assess the quality of cellulose nanofibrils (CNFs), ACS Sustain. Chem. Eng. 6 (9) (2018) 11959–11967. https://doi.org/10.1021/acssuschemeng.8b02278.

[33] X. Du, J. Qiu, S. Deng, Z. Du, X. Cheng, H. Wang, Alkylated nanofibrillated cellulose/carbon nanotubes aerogels supported form-stable phase change composites with improved *n*-alkanes loading capacity and thermal conductivity, ACS Appl. Mater. Interfaces. 12 (5) (2020) 5695–5703. https://doi.org/10.1021/acsami.9b17771.

[34] S. Salimian, M. Montazer, A.S. Rashidi, N. Soleimani, A. Bashiri Rezaie, PCM nanofibrous composites based on PEG/PVA incorporated by TiO_2/Ag nanoparticles for thermal energy management, J. Appl. Polym. Sci. 138 (46) (2021) 51357. https://doi.org/10.1002/app.51357.

[35] B. Wu, Y. Jiang, Y. Wang, C. Zhou, X. Zhang, J. Lei, Study on a PEG/epoxy shape-stabilized phase change material: Preparation, thermal properties and thermal storage performance, Int. J. Heat Mass Transf. 126 (2018) 1134–1142. https://doi.org/10.1016/j.ijheatmasstransfer.2018.05.153.

[36] L. Zhen, G. Meng, B. Zhou, W. Ma, Y. Yang, X. Duan, Y. Fu, H. Wang, Efficient utilization of interparticle mesopores in aluminosilicate towards thermal energy storage, J. Energy Storage. 36 (2021) 102359. https://doi.org/10.1016/j.est.2021.102359.

[37] C. Wang, L. Feng, W. Li, J. Zheng, W. Tian, X. Li, Shape-stabilized phase change materials based on polyethylene glycol/porous carbon composite: The influence of the pore structure of the carbon materials, Sol. Energy Mater Sol. Cells. 105 (2012) 21–26. https://doi.org/10.1016/j.solmat.2012.05.031.

[38] D.A. Gopakumar, A.R. Pai, Y.B. Pottathara, D. Pasquini, L. Carlos de Morais, M. Luke, N. Kalarikkal, Y. Grohens, S. Thomas, Cellulose nanofiber-based polyaniline flexible papers as sustainable microwave absorbers in the X-band, ACS Appl. Mater. Interfaces. 10 (23) (2018) 20032–20043. https://doi.org/10.1021/acsami.8b04549.

[39] H. Kono, T. Uno, H. Tsujisaki, T. Matsushima, K. Tajima, Nanofibrillated bacterial

cellulose modified with (3-Aminopropyl)trimethoxysilane under aqueous conditions: Applications to poly(methyl methacrylate) fiber-reinforced nanocomposites, ACS Omega. 5 (45) (2020) 29561–29569. https://doi.org/10.1021/acsomega.0c04533.

[40] S. Zhao, Z. Zhang, G. Sèbe, R. Wu, R.V. Rivera Virtudazo, P. Tingaut, M.M. Koebel, Multiscale assembly of superinsulating silica aerogels within silylated nanocellulosic scaffolds: Improved mechanical properties promoted by nanoscale chemical compatibilization, Adv. Funct. Mater. 25 (15) (2015) 2326–2334. https://doi.org/10.1002/adfm.201404368.

[41] Z. Liu, Y. Zhang, K. Hu, Y. Xiao, J. Wang, C. Zhou, J. Lei, Preparation and properties of polyethylene glycol based semi-interpenetrating polymer network as novel form-stable phase change materials for thermal energy storage, Energy Build. 127 (2016) 327–336. https://doi.org/10.1016/j.enbuild.2016.06.009.

[42] T. Xu, Y. Li, J. Chen, H. Wu, X. Zhou, Z. Zhang, Improving thermal management of electronic apparatus with paraffin (PA)/expanded graphite (EG)/graphene (GN) composite material, Appl. Therm. Eng. 140 (2018) 13–22. https://doi.org/10.1016/j.applthermaleng.2018.05.060.

[43] M. Wada, L. Heux, J. Sugiyama, Polymorphism of cellulose I family: Reinvestigation of cellulose IV, Biomacromolecules. 5 (4) (2004) 1385 – 1391. https://doi.org/10.1021/bm0345357.

[44] J. Gong, J. Li, J. Xu, Z. Xiang, L. Mo, Research on cellulose nanocrystals produced from cellulose sources with various polymorphs, RSC Adv. 7 (53) (2017) 33486–33493. https://doi.org/10.1039/C7RA06222B.

[45] X. Zhang, Z. Huang, B. Ma, R. Wen, M. Zhang, Y. Huang, M. Fang, Y. Liu, X. Wu, Polyethylene glycol/Cu/SiO_2 form stable composite phase change materials: Preparation, characterization, and thermal conductivity enhancement, RSC Adv. 6 (63) (2016) 58740–58748. https://doi.org/10.1039/C6RA12890D.

[46] W.-m. Guan, J.-h. Li, T.-t. Qian, X. Wang, Y. Deng, Preparation of paraffin/expanded vermiculite with enhanced thermal conductivity by implanting network carbon in vermiculite layers, Chem. Eng. J. 277 (2015) 56–63.

https://doi.org/10.1016/j.cej.2015.04.077.

[47] C.V. Podara, I.A. Kartsonakis, C.A. Charitidis, Towards phase change materials for thermal energy storage: Classification, improvements and applications in the building sector, Appl. Sci. 11 (4) (2021) 1490. https://doi.org/10.3390/app11041490.

[48] Ö. Gök, C. Alkan, Y. Konuklu, Developing a poly(ethylene glycol)/cellulose phase change reactive composite for cooling application, Sol. Energy Mater Sol. Cells. 191 (2019) 345–349. https://doi.org/10.1016/j.solmat.2018.11.038.

[49] Y. Yan, W. Li, R. Zhu, C. Lin, R. Hufenus, Flexible phase change material fiber: A simple route to thermal energy control textiles, Materials. 14 (2) (2021) 401. https://doi.org/10.3390/ma14020401.

[50] Y.-F. Shih, C.-H. Wang, M.-L. Tsai, J.-M. Jehng, Shape-stabilized phase change material/nylon composite based on recycled diatomite, Mater. Chem. Phys. 242 (2020) 122498. https://doi.org/10.1016/j.matchemphys.2019.122498.

[51] A. Karaıpeklı, A. Sarı, K. Kaygusuz, Thermal characteristics of paraffin/expanded perlite composite for latent heat thermal energy storage, Energy Source. Part A. 31 (10) (2009) 814–823. https://doi.org/10.1080/15567030701752768.

[52] C. Li, H. Yang, Expanded vermiculite/paraffin composite as a solar thermal energy storage material, J. Am. Ceram. Soc. 96 (9) (2013) 2793–2798. https://doi.org/10.1111/jace.12504.

[53] M. Senthilkumar, K.R. Balasubramanian, R.K. Kottala, S.P. Sivapirakasam, L. Maheswari, Characterization of form-stable phase-change material for solar photovoltaic cooling, J. Therm. Anal. Calorim. 141 (6) (2020) 2487–2496. https://doi.org/10.1007/s10973-020-09521-1.

[54] Q. Liu, W. Ren, F. Li, H. Cong, H.-M. Cheng, Synthesis and high thermal stability of double-walled carbon nanotubes using nickel formate dihydrate as vatalyst precursor, J. Phys. Chem. C. 111 (13) (2007) 5006–5013. https://doi.org/10.1021/jp068672k.

[55] H. Yang, R. Yan, H. Chen, D.H. Lee, C. Zheng, Characteristics of hemicellulose, cellulose and lignin pyrolysis, Fuel. 86 (12 – 13) (2007) 1781–1788. https://doi.org/10.1016/j.fuel.2006.12.013.

[56] D. Zou, X. Ma, X. Liu, P. Zheng, Y. Hu, Thermal performance enhancement of composite phase change materials (PCM) using graphene and carbon nanotubes as additives for the potential application in lithium-ion power battery, Int. J. Heat Mass Transf. 120 (2018) 33–41. https://doi.org/10.1016/j.ijheatmasstransfer.2017.12.024.

[57] X. Li, X. Sheng, Y. Guo, X. Lu, H. Wu, Y. Chen, L. Zhang, J. Gu, Multifunctional HDPE/CNTs/PW composite phase change materials with excellent thermal and electrical conductivities, J. Mater. Sci. Technol. 86 (2021) 171–179. https://doi.org/10.1016/j.jmst.2021.02.009.

[58] J. Lin, Y. Ouyang, L. Chen, K. Wen, Y. Li, H. Mu, Q. Ren, X. Xie, J. Long, Enhancing the solar absorption capacity of expanded graphite-paraffin wax composite phase change materials by introducing carbon nanotubes additives, Surf. Interfaces. 30 (2022) 101871. https://doi.org/10.1016/j.surfin.2022.101871.

[59] M.M. Umair, Y. Zhang, A. Tehrim, S. Zhang, B. Tang, Form-stable phase-change composites supported by a biomass-derived carbon scaffold with multiple energy conversion abilities. Ind. Eng. Chem. Res. 59 (4) (2020), 1393 – 1401. https://doi.org/10.1021/acs.iecr.9b06288.

[60] M.K. Hassanzadeh-Aghdam, M.J. Mahmoodi, M. Safi, Effect of adding carbon nanotubes on the thermal conductivity of steel fiber-reinforced concrete. Compos. B. Eng. 174 (2019) 106972. https://doi.org/10.1016/j.compositesb.2019.106972.

[61] S. Lv, Z. Qian, D. Hu, X. Li, W. He, A comprehensive review of strategies and approaches for enhancing the performance of thermoelectric module, Energies. 13 (12) (2020) 3142. https://doi.org/10.3390/en13123142.

[62] S. Ozbektas, B. Sungur, B. Topaloğlu, Performance analysis of thermoelectric generator at different hot surface temperatures, J. Thermophys. Heat Trans. 35 (4) (2021) 814 – 823. https://doi.org/10.2514/1.T6212.

Tables

Table 1. Detailed information of the materials used in the experiments.

Material	Specification	Role	Provider
BEKP	Commercial grade	CNF starting mateial	Moorim Paper Co., Ltd., Korea
APTMS	purity 97%	Silylation agent	Sigma-Aldrich, USA
MTMS	purity 98%	Silylation agent	Sigma-Aldrich, USA
Pw	Mw=436	Hydrophobic PCM	Sigma-Aldrich, USA
PEG	Mw=1000	Hydrophilic PCM	Sigma-Aldrich, USA
HCl	1 N, laboratory grade	PH regulator	Duksan Pure Chemicals Co., Ltd, Korea
Multiwalled CNTs	purity >95%, outer diameter 10–20 nm	Thermal conductivity enhancer	Research Nanomaterials, Inc., USA
Filter paper	Quantitative ashless, 11 cm in diameter	Leakage testing substrate	ADVANTEC, Japan

844 **Table 2.** PEG leakage percentage of different foam-stabilized composite PCMs.

Composite PCM	Weight before test (g)	Weight after test (g)	Weight of the leaked PEG (g)	Leakage percentage (%)
CNF-PEG	0.675	0.662	0.013	1.93
CNF_{APTMS}-PEG	0.47	0.462	0.008	1.70
CNF_{MTMS}-PEG	0.489	0.472	0.017	3.48

845

846 **Table 3.** Pw leakage percentage of different foam-stabilized composite PCMs.

Composite PCM	Weight before test (g)	Weight after test (g)	Weight of the leaked Pw (g)	Leakage percentage (%)
CNF-Pw	0.474	0.464	0.01	2.11
CNF_{APTMS}-Pw	0.431	0.419	0.012	2.78
CNF_{MTMS}-Pw	0.568	0.563	0.005	0.88

847

848 **Table 4.** The effect of CNF-based foams on the PCM absorption capacity and leakage
849 percentage.

Foam	Foam density (kg/m^3)	Foam porosity (%)	PCM absorption capacity (%)	PCM Leakage percentage (%)
CNF_{APTMS}-PEG	59.88	94.78	94.40	1.70
CNF_{APTMS}/CNT_{50}-PEG	67.26	94.52	93.63	1.81
CNF_{MTMS}-Pw	59.91	96.57	92.08	0.88
CNF_{MTMS}/CNT_{50}-Pw	64.53	96.39	91.77	1.71

850

851 **Table 5.** Melting points, freezing points and enthalpies of PEG-based PCM samples.

PCM sample	Heating process			Cooling process		
	Melting point (°C)	Enthalpy (kJ/kg)	Enthalpy reduction (%)	Freezing point (°C)	Enthalpy (kJ/kg)	Enthalpy reduction (%)
PEG	26.1	151.4	–	26.2	151.3	–
CNF_{APTMS}-PEG	25.2	144.2	4.76	25.6	144.3	4.63
CNF_{APTMS}/CNT_{50}-PEG	25.2	143.3	5.35	24.9	143.1	5.42

852

853 **Table 6.** Melting points, freezing points and enthalpies of Pw-based PCM samples.

PCM sample	Heating process			Cooling process		
	Melting point (°C)	Enthalpy (kJ/kg)	Enthalpy reduction (%)	Freezing point (°C)	Enthalpy (kJ/kg)	Enthalpy reduction (%)
Pw	57.7	202.8	-	55.5	202.7	-
CNF_{MTMS}-Pw	54.2	185.9	8.3	57.0	185.9	8.3
CNF_{MTMS}/CNT_{50}-Pw	53.4	184.6	9.0	57.2	184.5	9.0

854

855

856

857

858 **Captions**

859

860 **Fig. 1.** Schematic illustrating the solar-heat-electricity system based on novel PCM sandwich
861 structures.
862 **Fig. 2.** (a) Chemistry tuning of CNF using trimethoxy silane and the involved reaction
863 mechanism, (b) chemical structure of APTMS, and (c) chemical structure of MTMS.
864 **Fig. 3.** Effect of the chemical modifications of CNF foams on their PCM-stabilization effect:
865 leakage testing of (a) PEG-based composite PCMs and (b) Pw-based composite PCMs.
866 **Fig. 4.** TEM images of (a) CNF and (b) CNT; SEM images of (c) CNF_{APTMS}/CNT_{50} foam, (d)
867 CNF_{MTMS}/CNT_{50} foam, (e) CNF_{APTMS}/CNT_{50}-PEG composite and (f) CNF_{MTMS}/CNT_{50}-Pw
868 **Fig. 5.** Leakage testing of foam-stabilized composite PCMs on filter paper: (a) CNF_{APTMS}-
869 PEG, (b) CNF_{MTMS}-Pw, (c) CNF_{APTMS}/CNT_{50}-PEG and (d) CNF_{MTMS}/CNT_{50}-Pw.
870 **Fig. 6.** FT-IR spectra of (a) pristine CNF and chemically modified CNF, and (b) composite
871 PCMs and related components; XRD patterns of (c) pristine CNF and chemically modified
872 CNF, and (d) composite PCMs and related components.
873 **Fig. 7.** DSC curves of (a) PEG and PEG-based composite PCMs and (c) their curves after 100
874 cycles of melting and freezing; (b) Pw and Pw-based composite PCMs and (d) their curves
875 after 100 cycles of melting and freezing.
876 **Fig. 8.** Thermogravimetric curves of (a) PEG and PEG-based composite PCMs and (b) Pw
877 and Pw- based Composite PCMs.
878 **Fig. 9**. Temperature- heating time curves of (a) PEG based Composite PCMs and (b) Pw
879 based PCM under solar simulator, (c) thermal conductivity of PCM samples and (d) time
880 course of the open-circuit voltage of the thermoelectric generator with/without sandwich
881 PCMs on it.
882

Figures

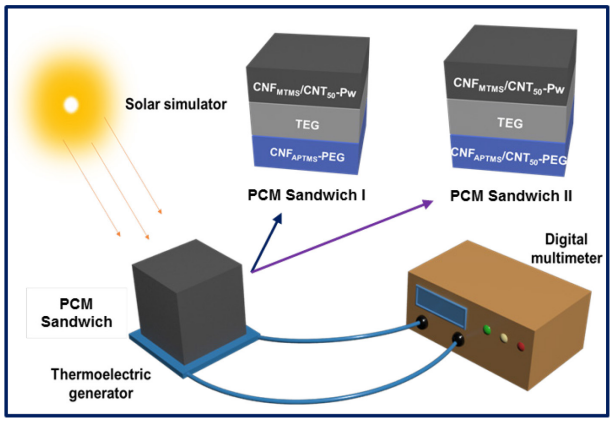

Fig. 1.

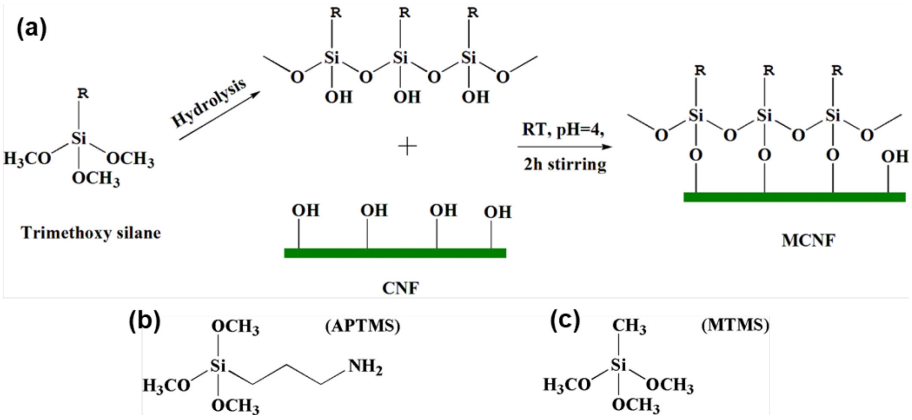

Fig. 2.

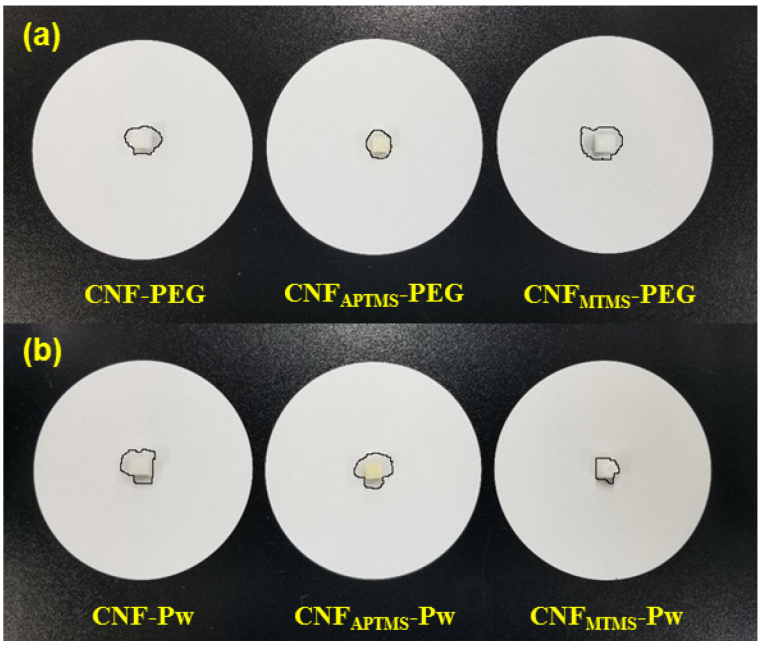

Fig. 3.

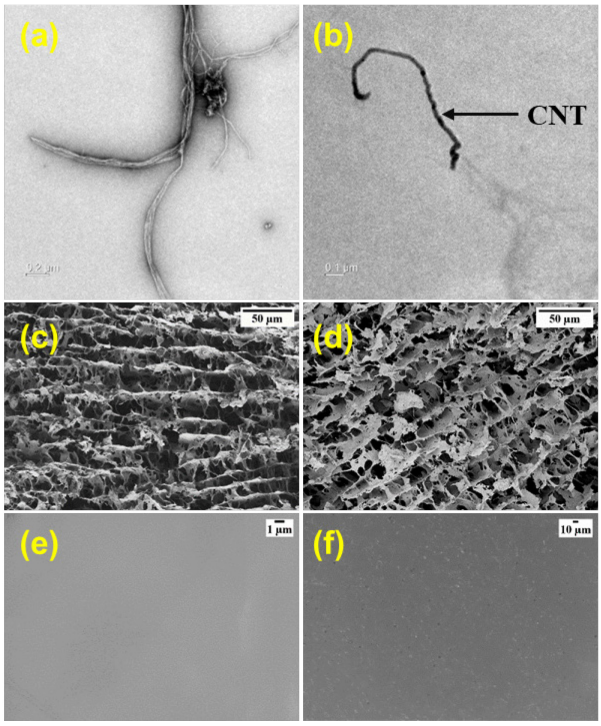

891

892 **Fig. 4.**

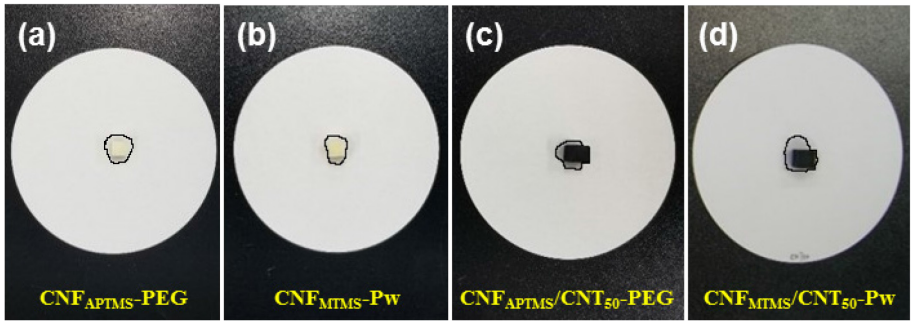

893

894 **Fig. 5.**

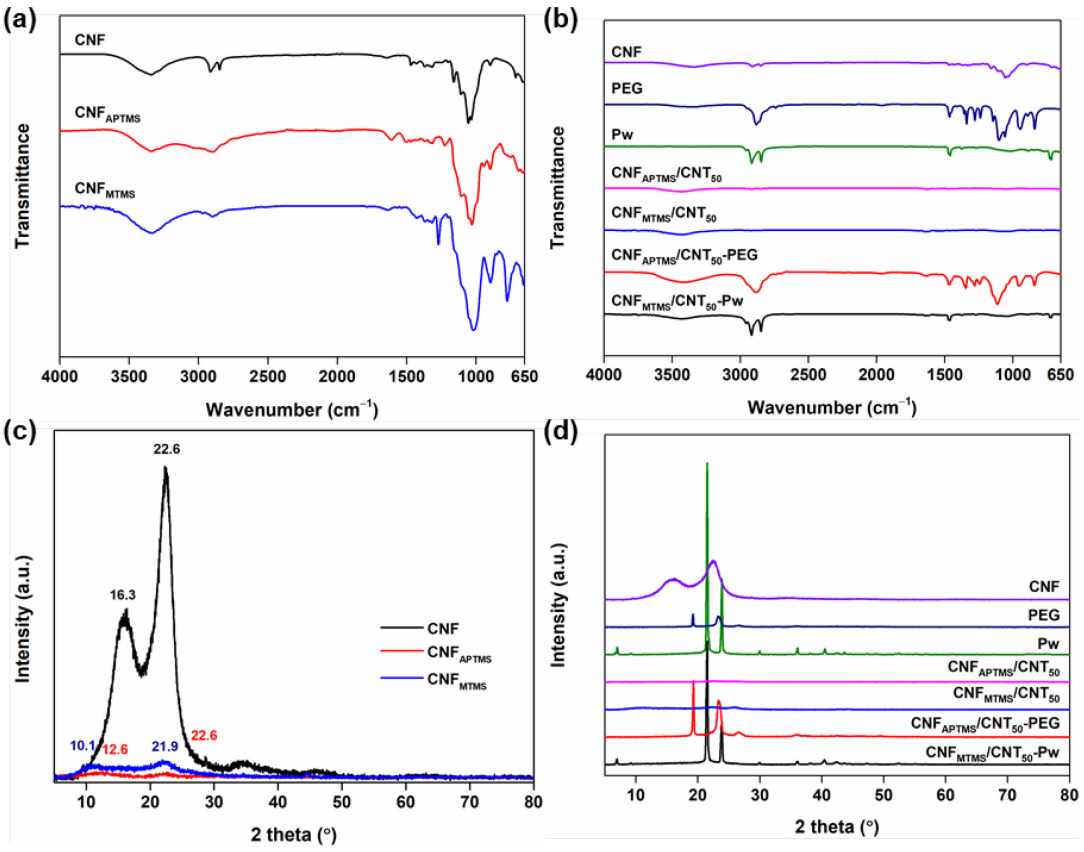

895

896 **Fig. 6.**

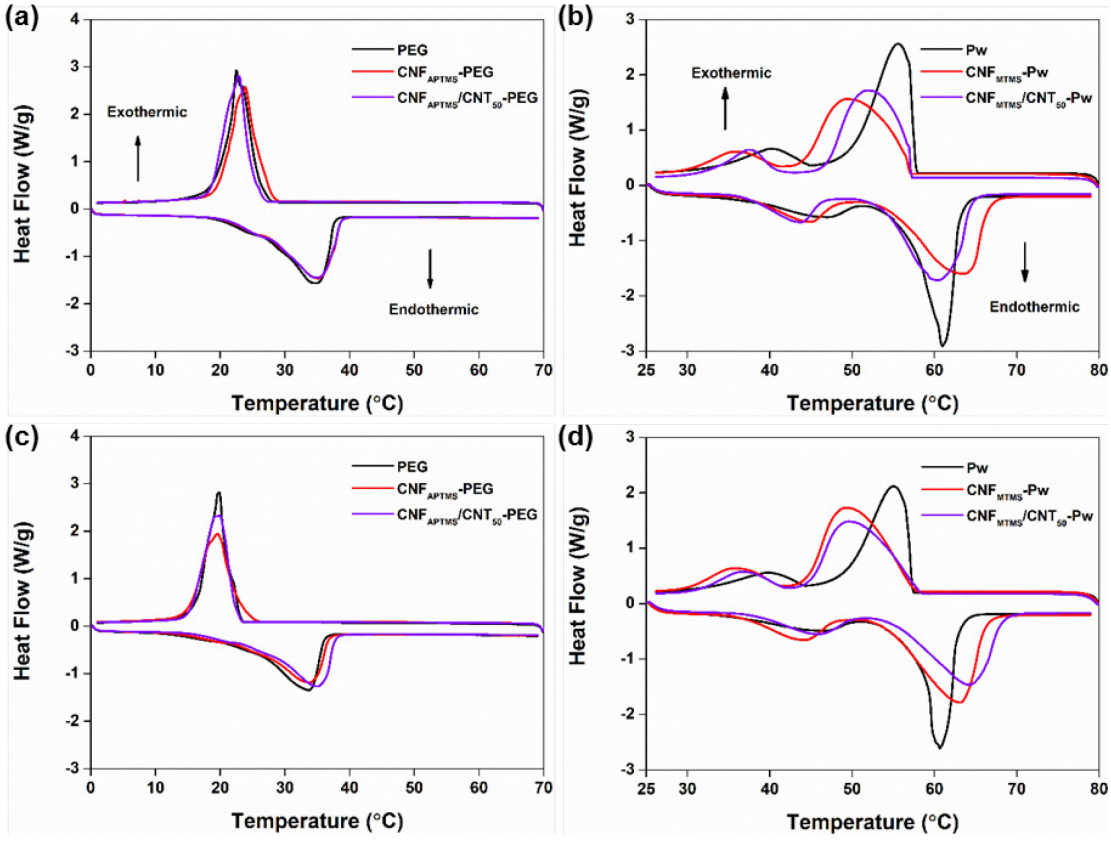

897

898 **Fig. 7.**

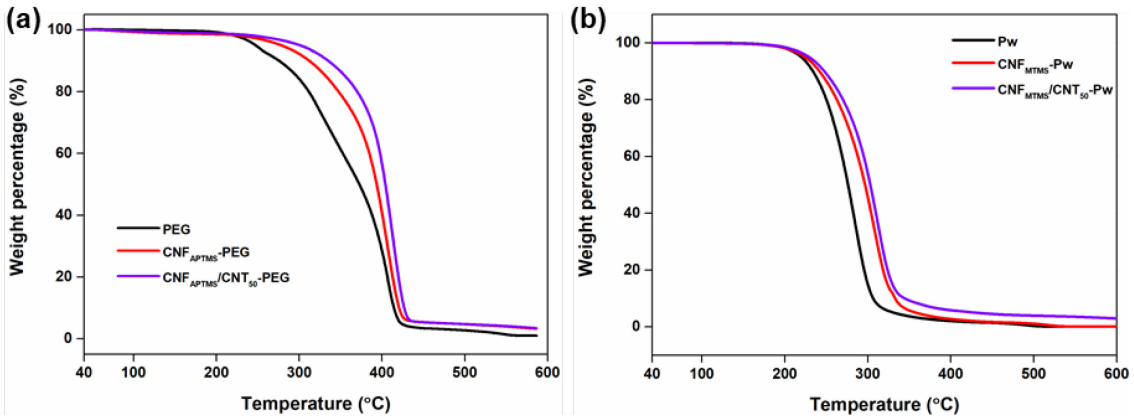

899

900 **Fig. 8.**

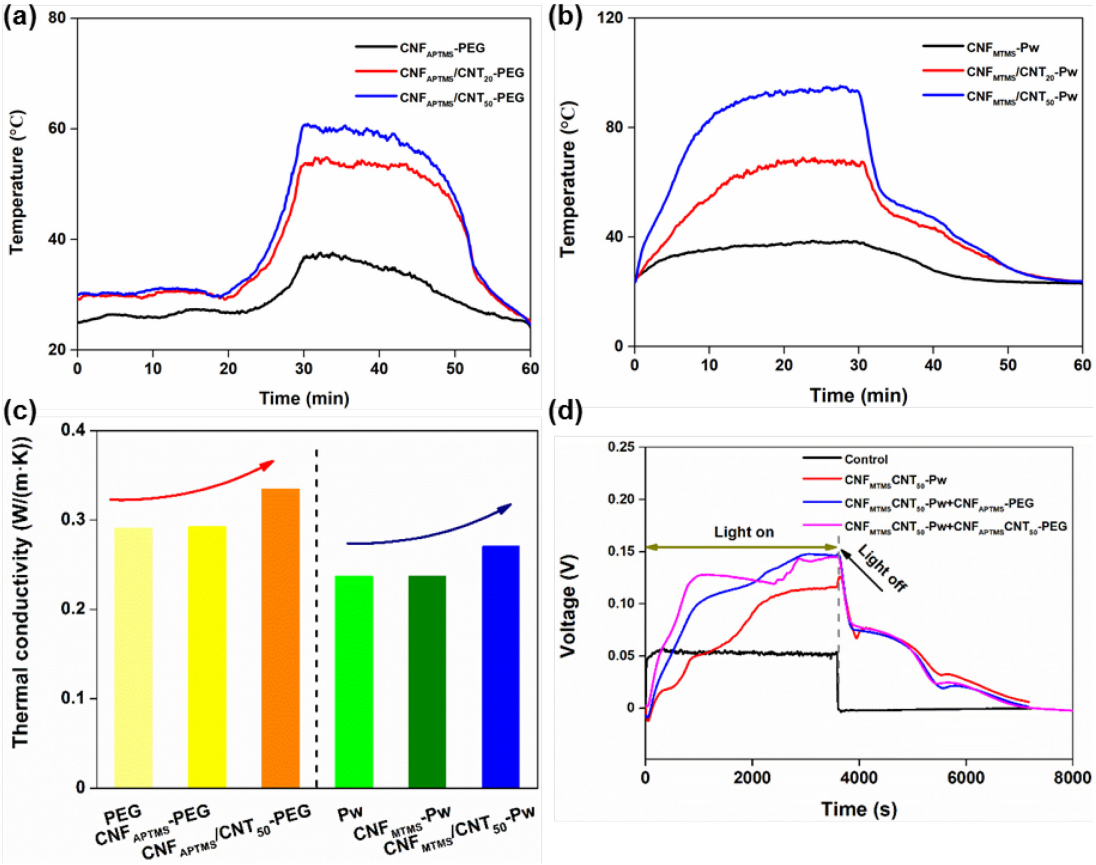

901

902 **Fig. 9**.